Lab on a Chip

INTERSTITIAL FLOW ENHANCES FORMATION, CONNECTIVITY, AND FUNCTION OF 3D BRAIN MICROVASCULAR NETWORKS GENERATED WITHIN MICROFLUIDIC DEVICE

Journal:	*Lab on a Chip*
Manuscript ID	LC-ART-07-2021-000605.R2
Article Type:	Paper
Date Submitted by the Author:	19-Nov-2021
Complete List of Authors:	Winkelman, Max; Northeastern University, Bioengineering Kim, Diana; Northeastern University, Bioengineering Kakarla, Shravani; Northeastern University, Bioengineering Grath, Alexander; Northeastern University, Bioengineering Silvia, Nathaniel; Northeastern University, Bioengineering Dai, Guohao; Northeastern University, Bioengineering

INTERSTITIAL FLOW ENHANCES FORMATION, CONNECTIVITY, AND FUNCTION OF 3D BRAIN MICROVASCULAR NETWORKS GENERATED WITHIN MICROFLUIDIC DEVICE

Max A. Winkelman[a], Diana Y. Kim[a], Shravani Kakarla[a], Alexander Grath[a], Nathaniel Silvia[a], and Guohao Dai[a*]

Affiliations

a. Department of Bioengineering, Northeastern University, Boston, MA, USA

*** Corresponding Author:**

Guohao Dai, Ph.D.
Associate Professor
Department of Bioengineering
Northeastern University
805 Columbus Ave, ISEC 224
Boston, MA 02115
g.dai@northeastern.edu
617-373-2207

Abstract

The bulk flow of interstitial fluid through tissue is an important factor in human biology, including the development of brain microvascular networks (MVNs) with the blood-brain barrier (BBB). Bioengineering perfused, functional brain MVNs has great potential for modeling neurovascular diseases and drug delivery. However, most *in vitro* models of brain MVNs do not implement interstitial flow during the generation of microvessels. Using a microfluidic device (MFD), we cultured primary human brain endothelial cells (BECs), pericytes, and astrocytes within a 3D fibrin matrix with (flow) and without (static) interstitial flow. We found that the bulk flow of interstitial fluid was beneficial for both BEC angiogenesis and vasculogenesis. Brain MVNs cultured under flow conditions achieved anastomosis and were perfusable, whereas those under static conditions lacked connectivity and the ability to be perfused. Compared to static culture, microvessels developed in flow culture exhibited enhanced vessel area, branch length and diameter, connectivity, and longevity. Although there was no change in pericyte coverage of microvessels, a slight increase in astrocyte coverage was observed in flow conditions. In addition, the immunofluorescence intensity of basal lamina proteins, collagen IV and laminin, was nearly doubled in flow culture. Lastly, the barrier function of brain microvessels was enhanced under flow conditions, as demonstrated by decreased dextran permeability. Taken together, these results highlighted the importance of interstitial flow in the *in vitro* generation of perfused brain MVNs with characteristics similar to those of the human BBB.

Keywords: *Brain Microvascular Networks, Interstitial Flow, Vasculogenesis, Angiogenesis, Blood-Brain Barrier, Microfluidic Devices*

1. Introduction

Brain microvascular networks (MVNs) are specialized vascular structures comprised of brain endothelial cells (BECs), pericytes (PCs), and astrocytes (ACs). BECs have upregulated expression of membrane transporters, such as glucose transporter 1 (GLUT1) and P-glycoprotein 1 (P-gp), as well as tight junction (ZO-1) and basement membrane (collagen IV and laminin) proteins(1). This contributes to a restrictive, semipermeable barrier between the blood and the brain extracellular space called the blood-brain barrier (BBB). PCs are mural cells that contact brain capillaries directly and modulate microvessel diameter and blood flow through contractile mechanisms(2,3). ACs are glial cells that extend processes which ensheathe brain blood vessels with perivascular endfeet. Both PCs and ACs provide paracrine and juxtacrine signals that enhance BBB-related gene and protein expression as well as barrier function(2,4). The physical and transport barrier created by the BBB is paramount for brain homeostasis. BBB dysfunction is a hallmark of most neurodegenerative diseases, including Alzheimer's disease(5), Parkinson's disease(6), Huntington's disease(7), amyotrophic lateral sclerosis(8), stroke(9), and brain cancers(10). The BBB is impermeable to 98% of small-molecule drugs and ~100% of large-molecule therapeutics, making it one of the largest obstacles to curative treatments of neurodegenerative diseases(11). It is postulated that the development of physiologically-accurate *in vitro* models of human brain MVNs will contribute to the understanding of the biological mechanisms of BEC microvessels and expedite the development of therapeutics for neurodegenerative diseases and brain cancers(12).

Microfluidic devices (MFDs) have become popular platforms for *in vitro* models of human physiology due to their precise spatiotemporal control over physical and chemical parameters. Several MFDs have been previously designed to study the human BBB and the cellular interactions that dictate its function(13–15). However, these designs implemented endothelial cell-lined fluidic channels and artificial, semipermeable membranes that did not accurately represent the natural morphology of brain microvasculature. At present, there are only two microfluidic models that developed brain MVNs through natural morphogenic processes (angiogenesis and vasculogenesis) by culturing endothelial cells with PCs and ACs within a 3D extracellular matrix (ECM)(16,17). These designs produced functional microvessels with diameters comparable to those of brain capillaries, arterioles, and venules (3 to 100 μm)(18,19). However, both studies relied exclusively on diffusion for the delivery of soluble growth factors and neglected to expose cells to physical

stimuli found in brain tissue, such as interstitial flow. Consequently, these MVNs were only perfused during permeability measurements and were not exposed to intravascular flow during the development of microvessels with open lumen.

Interstitial flow describes the bulk movement of fluid through the ECM of biological tissues. This bulk flow delivers nutrients, removes metabolic wastes, and provides mechanical cues to cells and the ECM. Mechanical signaling from interstitial flow governs cell behavior and protein expression(20,21). Indeed, interstitial flow has been shown to influence angiogenesis(22,23), vasculogenesis(24–26), lymphangiogenesis(27–29), glycocalyx formation(30,31), tumor cell migration(32,33), myofibroblast differentiation(34), inflammation(28), and embryogenesis(31,35). In the brain, the bulk flow of fluid through the interstitial space facilitates cross-talk between vascular and neural cells, long-distance transport of metabolites and regulatory peptides, and removal of harmful macroscopic wastes through the glymphatic system(36,37). Convection dominates the extracellular transport of soluble factors through 3D ECMs and effectively governs the local gradients of diffusible signals(38). For example, interstitial flow has been shown to act synergistically with vascular endothelial growth factor (VEGF) to direct capillary branching through a morphogen gradient amplification mechanism(39). In previous MFD models, interstitial flow was induced to develop self-assembled MVNs using endothelial cells and fibroblasts from non-brain sources(22–26,40,41). In some models, the same mechanism that induced interstitial flow also promoted the perfusion of microvessels once anastomosis was achieved(24,25). In addition to the exchange of metabolites and gases, blood flow in vessels provides shear stress and strain to the vascular wall which modulates vascular function(42,43). Indeed, intravascular flow regulates shear stress-responsive genes and can alter endothelial cell structure(44,45). Shear stress also has a direct effect on the differentiation of vascular endothelial cells towards a BBB phenotype(46). Due to their significant role in vascular morphogenesis, interstitial and luminal flow should be included in microfluidic models attempting to recapitulate brain microvasculature.

Recently, the effect of interstitial flow on the brain microvessel formation was explored in a Transwell-based system by Figarol and colleagues(47). Despite the development of brain MVNs cultured under continuous interstitial flow, it was observed that microvessels oriented themselves perpendicular to shear flow. As a result, the authors stated that these microvessels were non-perfused and found no significant differences in the mean vessel diameter between cultures with

and without flow(47). In our study, we cultured primary human BECs, PCs, and ACs within a MFD to develop brain MVNs through both angiogenic and vasculogenic processes. Microvessels were cultured with (flow condition) or without (static condition) interstitial flow induced by a hydrostatic pressure gradient across a 3D fibrin hydrogel. Our overarching hypothesis was that interstitial flow would improve brain MVN formation and interconnectivity as well as enhance endothelial barrier function. MVNs were evaluated by their morphological features, longevity, perfusion, cellular interactions, protein expression, and permeability. Our work highlights the importance of the bulk flow of interstitial fluid for *in vitro* brain MVN development and provide a practical approach to increase the success rate of achieving perfusable vasculature in MFD.

2. Materials and Methods

2.1 Cell Culture

Endothelial Cell Growth Medium 2 (EGM-2) was made by combining Growth Medium 2 (PromoCell) with Growth Medium 2 SupplementMix and 1% penicillin/streptomycin (Fisher Scientific). Pericyte medium and astrocyte medium were created by combining pericyte and astrocyte basal medium (ScienCell) with pericyte and astrocyte growth supplement, respectively, and then adding 2% fetal bovine serum and 1% antibiotic solution. Primary human brain microvascular endothelial cells (BECs, ScienCell, Cat: 1000) were expanded in EGM-2 on tissue culture flasks coated with 0.2% porcine gelatin (Sigma-Aldrich). To visualize cells in culture, BECs were made to express tandem dimer Tomato fluorescent protein (tdTomato, Vector Builder, VB181014-1005thm) or enhanced green fluorescent protein (EGFP, Vector Builder, VB150915-10026) using lentiviral transduction protocols. Briefly, 18 hours after seeding, BECs were cultured in EGM-2 containing 5 μg/mL polybrene (Vector Builder) and the manufacturer's recommended concentration of either tdTomato or EGFP lentiviruses. After 24 hours, the medium was replaced with normal EGM-2. On Day 3, cell selection was performed by adding EGM-2 with 10 μg/mL blasticidin or puromycin (Sigma-Aldrich). Unmodified BECs, BECs expressing tdTomato (BECs-tdT), and BECs expressing EGFP (BECs-EGFP) were expanded in EGM-2 and harvested between passage 5 and 6. Primary human brain vascular pericytes (PCs, ScienCell, Cat: 1200) and human astrocytes (ACs, ScienCell, Cat: 1800) were expanded in pericyte and astrocyte medium, respectively, on tissue culture flasks coated with poly-L-lysine (ScienCell) and harvested between

passage 2 and 5. All cells were incubated at 37°C and 5% CO_2 and harvested at 70% confluence using 0.25% trypsin-EDTA (Fisher Scientific).

2.2 Characterization of interstitial flow in microfluidic device

3D Cell Culture Chips from AIM Biotech (Singapore) were used for all experiments. These MFDs possessed one central hydrogel channel flanked by two fluidic channels connected to cell culture medium reservoirs (Fig. 1A). To quantify interstitial flow in the MFD, we first injected a fibrin solution into the hydrogel channel. Briefly, fibrinogen (8 mg/mL) and thrombin (4 U/mL) from bovine serum (Sigma-Aldrich) were dissolved in EGM-2 and phosphate-buffered saline (PBS) with calcium and magnesium ions (Fisher Scientific), respectively. Fibrinogen and thrombin solutions were combined at equal volumes to produce a fibrin solution with a final concentration of 4 mg/mL. Fibrin solutions were quickly added to hydrogel channels and allowed to polymerize for at least 10 minutes at room temperature.

Interstitial flow across the hydrogel channel was generated by creating a hydrostatic pressure difference between opposite reservoirs. To simulate how cell culture medium would flow across the fibrin matrix, the permeability of the fibrin hydrogel was needed. Since the change in reservoir volume over time was difficult to measure accurately, fluorescent dextran solution was used to visualize the movement of fluid across the fibrin gel. Briefly, Oregon Green™ 488 dextran (70 kDa, Invitrogen) was dissolved in EGM-2 to produce a 5 μg/mL solution. Different volumes of dextran solution and normal EGM-2 were added to each "high-pressure" and "low-pressure" reservoir, respectively, as shown in Table 1. These volumes produced five differential pressures across the fibrin hydrogel: 0, 0.375, 0.75, 1.125, and 1.5 mmH_2O. Pressure values (mmH_2O) were assumed to be equal to the volume height difference (mm) between opposite reservoirs. Immediately afterwards, time-lapse fluorescence images were acquired every 10 seconds for 5 minutes using an Eclipse Ti2 inverted microscope (Nikon) with a 4X objective at 37°C. Fluorescence images were analyzed in ImageJ (National Institute of Health) to calculate the permeability of the fibrin gel and simulate interstitial flow in the microfluidic device (Supplementary Methods S.1). Once bulk fluid movement across the hydrogel channel was properly characterized, we sought to determine the influence of interstitial flow on brain microvascular network development and function. For all future experiments, cells were cultured

under either static or flow conditions where a hydrostatic pressure difference of 0 or 1.5 mmH_2O was established, respectively (Fig. 1B).

2.3 Brain endothelial cell angiogenesis

To determine the influence of interstitial flow on angiogenesis, BECs-EGFP were stimulated to extend angiogenic sprouts into the hydrogel channel. Briefly, solutions of fibrinogen (8 mg/mL) and thrombin (4 U/mL) were prepared as previously described (Materials and Methods 2.2). PCs and ACs were harvested and resuspended together in the fibrinogen solution at 4×10^6 cells/mL each. Fibrinogen-cell and thrombin solutions were combined at a ratio of 1:1 and introduced to the hydrogel channel of MFDs and allowed to polymerize for 10 minutes at room temperature. The final fibrin concentration was 4 mg/mL. The final cell concentration of both PCs and ACs was 2×10^6 cells/mL. To create vascular channels from which angiogenic sprouts would originate, BECs-EGFP were harvested and side-seeded in one of the fluidic channels. BECs-EGFP were resuspended in EGM-2 at 5×10^6 cells/mL and introduced to the low-pressure fluidic channel. MFDs were inverted 90° and incubated (37°C and 5% CO_2) for 15 minutes to encourage BECs to adhere to the fibrin gel interface. Afterwards, non-adherent cells were washed out of the fluidic channel with EGM-2. All cells were cultured in MFDs for 7 days with EGM-2 with 50 ng/mL of recombinant human VEGF (PeproTech, Cat: 100-20) and 5 μg/mL of bovine aprotinin (Fisher Scientific). VEGF and aprotinin were supplemented to promote angiogenesis and prevent significant fibrin degradation, respectively. Samples were cultured at 37°C and 5% CO_2 under static (0 mmH_2O) or flow (1.5 mmH_2O) conditions as previously described (Materials and Methods 2.2). Every 24 hours, old cell culture medium was removed from reservoirs and replaced with fresh medium to reestablish volumes.

2.4 Brain endothelial cell vasculogenesis

To determine the influence of interstitial flow on vasculogenesis, BECs-tdT or BECs-EGFP were stimulated to form MVNs in the hydrogel channel. Briefly, solutions of fibrinogen (8 mg/mL) and thrombin (4 U/mL) were prepared as previously described (Materials and Methods 2.2). BECs, PCs, and ACs were harvested and resuspended together in the fibrinogen solution at 10×10^6, 2×10^6, and 2×10^6 cells/mL, respectively. Fibrinogen-cell and thrombin solutions were combined at a ratio of 1:1 and introduced to the hydrogel channel of MFDs and allowed to

polymerize for 10 minutes at room temperature. The final fibrin concentration was 4 mg/mL. The final cell concentrations of BECs, PCs, and ACs, were 5×10^6, 1×10^6, and 1×10^6 cells/mL, respectively. Cells were cultured for 3 days in EGM-2 with VEGF (50 ng/mL) and aprotinin (5 μg/mL). On Day 3, BECs-tdT or BECs-EGFP were side-seeded in both of the fluidic channels, as previously described (Materials and Methods 2.3), to increase the chance of anastomosis. From this point on, cells were cultured in EGM-2 with just aprotinin for up to 14 days in culture. VEGF supplementation was not continued to promote the formation of endothelial tight junctions and decrease vascular permeability(48). Cells in MFDs were cultured at 37°C and 5% CO_2 under static (0 mmH_2O) or flow (1.5 mmH_2O) conditions as previously described (Materials and Methods 2.2). Every 24 hours, old cell culture medium was removed from reservoirs and replaced with fresh medium to reestablish volumes.

2.5 Immunocytochemistry protocol

Immunocytochemistry techniques were used to fluorescently label specific proteins at the conclusion of cell culture. Briefly, all samples were washed three times with PBS and fixed with 4% paraformaldehyde (Alfa Aesa) for 1 hour at room temperature. Next, samples were washed three times with PBS and incubated with a blocking/permeabilizing (B/P) solution comprised of 10% normal goat serum (MP Biomedicals), 0.2% Triton X-100 (Fisher Scientific), and 0.1M glycine (Fisher Scientific) in PBS overnight at 4°C. Samples were then incubated with primary antibodies in B/P solution overnight at 4°C. PCs and ACs were labeled with neural/glial antigen 2 (NG-2) and glial fibrillary acidic protein (GFAP), respectively. BEC tight junctions were labeled with zonula occludens-1 (ZO-1). The basal lamina of microvessels was identified with collagen IV and laminin. Membrane transporters on BECs, PCs, and ACs were identified with GLUT1 and P-gp. After primary antibody incubation, samples were washed three times with PBS and then incubated with secondary antibodies and Hoechst 33342 (1:1000, Invitrogen) in B/P solution overnight at 4°C. Afterwards, samples were washed three times with PBS and stored at 4°C until needed. Specific antibody information can be found in Supplementary Tables 1 and 2.

2.6 Angiogenic sprout analysis

BECs-EGFP were allowed to sprout into the fibrin gel containing PCs and ACs for one week under static or flow culture conditions. Fluorescence z-stack (200 μm range using 10 μm

slices) images were acquired on Day 1, Day 3, and Day 7 using an Eclipse Ti2 microscope with a 20X objective. Angiogenic sprouts were identified by the EGFP signal expressed in BECs. In ImageJ, z-stacks were compressed to maximum intensity projections (MIPs). Regions of interest (ROIs) were selected to identify angiogenic sprouts originating from three adjacent hydrogel-liquid interfaces located between microposts. For Days 1, 3, and 7, the number of angiogenic sprouts in each ROI were counted. For these sprouts, sprout length was measured as the Euclidean distance between the base of the micropost and the sprout tip. On Day 7, sprout diameter was measured as the width of angiogenic sprouts located at the tip of microposts (230 μm into the hydrogel channel). Sprout length and diameter were averaged for each ROI. For sprout count, average length, and average diameter, 3 experimental replicates were analyzed to generate mean values for static and flow culture conditions. After imaging was completed, all samples were fixed and stained for NG-2 and GFAP to collect representative images.

2.7 Microvessel perfusion

Fluorescent microspheres were used to determine if the MVNs formed from BECs-tdT, PCs, and ACs under static and flow conditions were perfusable. After 8 days in culture, Dragon Green polystyrene microspheres (1.9 μm diameter, Bang Laboratories, 1:1000) were resuspended in warm (37°C) EGM-2. For all samples, 70 μL of microsphere solution was added to both of the high-pressure reservoirs and 50 μL of warm EGM-2 was added to both of the low-pressure reservoirs, producing a hydrostatic pressure difference of 0.75 mmH_2O. This stimulated microspheres to enter open lumen at the hydrogel-liquid interface. A pressure difference of 0.75 mmH_2O was selected to simulate what MVNs experienced when 50% of the original pressure difference was present and to measure intraluminal flow velocities closer to the average values experienced by microvessels. Immediately after adding the microsphere solution, fluorescence time lapse images (300 millisecond intervals for 30 seconds) were acquired using an Eclipse Ti2 microscope at 37°C with a 10X objective (Supplementary Videos 1 and 2). One minute after the microsphere solution was added, representative fluorescence images of the hydrogel channel were acquired with a 4X objective. Anastomosis was considered achieved if the microspheres were observed flowing from the high-pressure channel to the low-pressure channel exclusively through the lumen of microvessels. The movement of microspheres through MVNs cultured in static and

flow conditions was analyzed to determine microsphere velocity and estimate microvessel shear stress (Supplementary Methods S.2).

2.8 Microvessel analysis

BECs-tdT, PCs, and ACs formed brain MVNs when cultured under both static and flow conditions. Microvessel analysis was performed to quantify the effect of interstitial flow on MVN characteristics. After 8 days in culture, all samples were fixed as previously described (Materials and Methods 2.5). Fluorescence z-stack (50 μm range at 5 μm intervals) images were acquired using a LSM 800 confocal laser scanning microscope (ZEISS) with a 20X objective. Microvessels were identified by the tdTomato signal expressed in BECs. This signal was used to calculate blood vessel parameters (blood vessel area, branch number, average branch length, average branch diameter, and the number of blood vessel segments) for MVNs cultured under static and flow conditions (Supp. Fig. 2). First, in ImageJ, z-stacks were compressed to MIPs. Next, the tdTomato signal was converted to a binary image and individual particles smaller than an individual BEC were removed. Binary images were then used to determine the vessel area, A_V, as well as vessel area as a percentage of the total area of the image. The ImageJ plugin, Skeletonize, was used to skeletonize the binary image and Analyze Skeleton (2D/3D) was used to determine the number of branches, n_B, and the average branch length, L_B. From these values, average branch diameter, D_B, was calculated using the following equation:

$$D_B = \frac{A_V}{n_B \times L_B} \quad (1)$$

Analyze Skeleton was also used to determine the number of blood vessels segments of each sample by counting the Skeleton ID numbers assigned in each image. For all blood vessel parameters, 6 experimental replicates were analyzed to generate average values for static and flow conditions.

To determine the effect of interstitial flow on MVN longevity, BECs-EGFP, PCs, and ACs were cultured under static or flow conditions for 14 days. Samples were fixed on Day 8 and Day 14. Fluorescence z-stack (50 μm range at 5 μm intervals) images were acquired using a LSM 800 confocal microscope with a 20X objective. In ImageJ, the EGFP signal was used to measure blood vessel area, average branch diameter, and the number of blood vessel segments for MVNs cultured under static and flow conditions. For all parameters, 6 experimental replicates were analyzed. For both static and flow cultures, Day 8 averages were compared to Day 14 averages.

2.9 Pericyte and astrocyte analysis

To determine the effect of interstitial flow on the association of PCs and ACs with microvessels, BECs-tdT, PCs, and ACs were cultured under static or flow conditions for 8 days. In all samples, PCs and ACs were immunocytochemically labeled with NG-2 and GFAP, respectively. Fluorescence z-stack (50 μm range at 5 μm intervals) images were acquired using a LSM 800 confocal microscope with a 20X objective. Microvessels were identified using the tdTomato signal. When measuring PC and AC coverage, z-stack images were cropped at one slice (5 um) from the top and bottom of the microvessels imaged. This was to minimize the inclusion of PCs and ACs in the fibrin hydrogel that were not directly contacting the blood vessels. In ImageJ, cropped z-stacks were compressed into MIPs and binary images were made of the tdTomato, NG-2, and GFAP channels. PC and AC coverage was calculated as the area of overlap of the tdTomato signal with the NG-2 and GFAP signal, respectively. Both values were represented as a percentage of the total microvessel area. When measuring the number of GFAP+ ACs and the total length of AC process extensions, full-range z-stacks were compressed into MIPs. The number of GFAP+ ACs was calculated by counting the number of nuclei associated with the GFAP signal. Next, the binary GFAP signal was skeletonized, and Analyze Skeleton (2D/3D) was used to calculate the total length of AC processes extended into the fibrin hydrogel. For all parameters, 6 experimental replicates were analyzed to generate average values for static and flow conditions.

2.10 Protein immunofluorescence analysis

To determine the effect of interstitial flow on MVN protein expression, BECs-tdT, PCs, and ACs were cultured under static or flow conditions for 8 days. On Day 8, all samples were fixed and stained for ZO-1, laminin, and collagen IV. Fluorescence z-stack (50 μm range at 5 μm intervals) images were acquired using a LSM 800 confocal microscope with a 20X objective. In ImageJ, z-stacks were compressed into MIPs. The tdTomato signal was used to identify microvessels and calculate vessel area as previously explained (Materials and Methods 2.8). ROIs were selected to include microvessels with clearly defined borders. In each ROI, the total pixel intensity value for each fluorescently tagged protein was measured. The total pixel intensity was then normalized by microvessel area to allow for statistical analysis. For all protein intensity analysis, 6 experimental replicates were analyzed to generate average values for static and flow

conditions. Average values measured for microvessels cultured under flow conditions were represented relative to the averages measured under static conditions.

2.11 Enzyme-linked immunosorbent assay

To determine the effect of interstitial flow on the secretion of soluble signals from MVNs, normal BECs, PCs, and ACs were cultured under static or flow conditions for 6 days. Brain-derived neurotrophic factor (BDNF) was selected as the target protein for enzyme-linked immunosorbent assay (ELISA). To ensure sufficient BDNF would be detected, two modifications were made to the vasculogenesis protocol. First, the final cell densities of BECs, PCs, and ACs were increased to 6×10^6, 2×10^6, and 2×10^6 cells/mL, respectively. Second, culture medium was changed every other day. On days between medium changes, the reservoir volumes required for static and flow conditions were reestablished using the conditioned medium. The entire volume from all reservoirs was collected from samples on Day 2, 4, and 6 and stored at -80°C until needed. Concentrations of soluble human BDNF in conditioned media were determined using Total BDNF Quantikine ELISA Kit (R&D Systems) according to the manufacturer's instructions. For BDNF concentrations, the culture medium volumes of 3 MFDs were analyzed in duplicate to generate average values for static and flow conditions on each day.

2.12 Dextran permeability assay

To determine the effect of interstitial flow on microvessel permeability, BECs-EGFP, PCs, and ACs were cultured under static or flow conditions for 8 days. On Day 8, a 5 μg/mL solution of Texas Red™ 594 dextran (70 kDa, Invitrogen) was prepared in warm EGM-2. For all samples, 60 μL of warm EGM-2 was added to both low-pressure reservoirs and then 60 μL of dextran solution was quickly added to both high-pressure reservoirs. Fluorescence z-stack (50 μm range at 5 μm intervals) time lapse (30 second intervals for a maximum of 180 seconds) images were acquired using a LSM 880 confocal laser scanning microscope at 37°C with a 20X objective. Due to the brief imaging period, CO_2 and humidity levels were not regulated. For MVNs cultured under both static and flow conditions, ROIs were selected to include microvessels with well-defined borders. In ImageJ, z-stacks for each time point were compressed into MIPs. It was assumed that dextran fluorescence intensity increased proportionally with the concentration of dextran and that the microvessels analyzed were circular. With those assumptions, microvessel permeability

coefficients (P) were calculated using the following equation derived from Fick's First Law by Uwamori and colleagues(49):

$$P = \frac{r}{2} \times \frac{\frac{dI}{dt}}{I_0} \quad (2)$$

where r is the radius of the microvessel, $\frac{dI}{dt}$ is the change over time of the fluorescence intensity of the Texas Red dextran in the extracellular space within 5 μm of the microvessel wall, and I_0 is the initial fluorescence intensity of the intraluminal dextran, which was constant throughout imaging. For dextran permeability experiments, 9 experimental replicates were analyzed to generate average values for static and flow conditions.

2.13 Statistical analysis

All statistical analysis was performed using Prism (GraphPad Software). Statistical testing between two experimental conditions was done using a two-tailed Student's t-test with Welch's correction. Statistical testing of data with more than one experimental variable was done using two-way analysis of variance with Šidák multiple comparisons test. Statistical significance was determined as $p < 0.05$. All data are represented as the mean with error bars of the standard error of mean (SEM).

3. Results

3.1 Characterizing interstitial flow across the fibrin hydrogel

3D Cell Culture Chips from AIM Biotech (Fig. 1A) were selected for experimentation due to their ability to generate interstitial flow across a hydrogel channel by creating a hydrostatic pressure gradient between opposite reservoirs. We selected the pressure differences of 0 and 1.5 mmH_2O to represent the static and flow culture conditions, respectively, for all experiments (Fig. 1B). A solution of Oregon Green dextran (70kDa) was employed to visualize the bulk flow of fluid across the central channel and to calculate the permeability of the fibrin hydrogel. Under static conditions, the dextran solution remained in the fluid channel and did not diffuse significantly into the fibrin hydrogel during imaging (Fig. 1C). Under flow conditions, the dextran solution migrated across the fibrin hydrogel from the high-pressure channel and reached the low-pressure channel after approximately 180 seconds (Fig. 1C). We assumed that the movement of fluorescent dextran across the hydrogel channel would be similar to that of other solutes in the culture medium. During flow culture, the volume height difference between opposite reservoirs decreases until equilibrium is reached. Therefore, to better characterize the interstitial flow experienced as reservoir volumes equilibrated, various volumes were added to reservoirs to produce hydrostatic pressures from 0 and 1.5 mmH_2O (Table 1) and the dextran solution velocity was measured. The hydrostatic pressure differences of 0, 0.375, 0.75, 1.125, and 1.5 mmH_2O generated average dextran solution velocities of 0.08 ± 0.02, 1.73 ± 0.07, 3.64 ± 0.15, 4.74 ± 0.07, and 5.73 ± 0.10 μm/s (Fig. 1D), respectively, which corresponded to average dextran solution flow rates of 0.22 ± 0.05, 4.54 ± 0.18, 9.55 ± 0.39, 12.44 ± 0.19, 15.03 ± 0.26 nL/s (Fig. 1E), respectively. The average volumetric flow rates calculated at 0.375, 0.75, 1.125, and 1.5 mmH_2O were then used to calculate the average fibrin hydrogel permeability of $4.35 \pm 0.23 \times 10^{-13}$ m^2. Using this permeability value, we were able to simulate the interstitial flow velocity (Fig. 1F) and volumetric flow rate (Fig. 1G) that would be experienced across the fibrin hydrogel over time under flow conditions. Both the interstitial velocity and flow rate decreased exponentially from their initial values and had reduced by three orders of magnitude after approximately 9 hours. Despite the decay in interstitial flow values, we postulated that the presence of the interstitial flow would markedly influence BEC morphogenesis compared to the absence of flow. Hence, to determine the effect of interstitial flow on microvessel development and function, we compared the differences between MVNs generated under the static and flow conditions described above.

3.2 Interstitial flow enhanced brain endothelial cell angiogenesis

To determine the influence of interstitial flow on BEC angiogenesis, BECs-EGFP were side-seeded along one fluidic channel and sprouted into the fibrin gel containing PCs and ACs under static or flow culture conditions (Fig. 2A). Under both conditions, BECs-EGFP produced angiogenic sprouts that extended into the fibrin hydrogel over the course of a week (Fig. 2B). In the flow condition, BECs extended angiogenic sprouts against the direction of interstitial flow. By Day 7, angiogenic sprouts were surrounded by supporting NG-2+ PCs and GFAP+ ACs in both conditions (Fig. 2C). After one day in culture, there was no significant difference between the number of sprouts or the average sprout length for BECs-EGFP cultured under static and flow conditions. However, on Day 3 and Day 7, both the sprout count (Fig. 2D) and average length (Fig. 2E) were enhanced for BECs-EGFP cultured under flow compared to static conditions. The Day 7 sprout count observed under static and flow conditions was 8.00 ± 1.53 and 16.00 ± 0.58, respectively (Fig. 2D). The Day 7 average sprout length observed under static and flow conditions was 294.36 ± 13.47 and 560.11 ± 10.11 μm, respectively (Fig. 2E). Finally, the Day 7 average sprout diameter observed under static and flow conditions was 13.64 ± 0.43 and 39.61 ± 2.28 μm, respectively (Fig. 2F). In summary, the mean sprout count, average length, and average diameter were increased for BECs-EGFP cultured under flow conditions compared to static conditions. Taken together, these data indicate that the application of interstitial flow enhances BEC angiogenesis.

3.3 Interstitial flow engendered brain microvascular network perfusion

To determine the influence of interstitial flow on brain MVN formation, BECs-tdT, PCs, and ACs were suspended in a fibrin gel and cultured under static or flow conditions (Fig. 3A). After two days in culture, BECs-tdT in both culture conditions began to expand into the fibrin matrix and form vascular plexuses (Fig. 3B). On Day 3, additional BECs-tdT were side-seeded in both fluidic channels to increase the chance of anastomosis across the hydrogel channel. By Day 8, mature 3D brain MVNs supported by NG-2+ PCs and GFAP+ ACs were formed within the hydrogel channel under both conditions (Fig. 3B). These MVNs were observed throughout the entire length of the hydrogel channel in static and flow samples, indicating that significant degradation and regression of the fibrin gel had not occurred (Supp. Fig. 1). BECs-tdT side-seeded in fluidic channels had formed confluent monolayers, creating an endothelial barrier between the

fluidic channels and the fibrin gel (Fig. 3C). After 8 days, microvessels formed under both static and flow culture conditions expressed tight junction protein, ZO-1, at the periphery of BECs (Fig. 3D). Collectively, these observations demonstrated that BECs-tdT were able to undergo endothelial morphogenic processes to form 3D MVNs within a MFD, similar to previous studies(16,50,51). Further analysis was performed to elucidate the distinctions between the microvessel networks formed under the two culture conditions.

Microvessel perfusion and anastomosis was visualized with fluorescent microspheres. After 8 days of static or flow culture, a solution of 1.9 μm diameter microspheres was added to MFD reservoirs such that the hydrostatic pressure difference across the fibrin gel was 0.75 mmH_2O (Fig. 4A). This stimulated microspheres to flow from the high-pressure channel to the low-pressure channel through the open lumen of microvessels. However, we did not observe MVN anastomosis in any sample cultured under static conditions. While microspheres were able to enter several open lumens formed in static culture, they were not able to make egress and terminated in microvessels in the hydrogel channel. In addition, microspheres were also observed in the interstitial space of the fibrin hydrogel in static samples (Fig. 4B, Supp. Vid. 1). This demonstrated that microvessels were porous enough to allow the exit of microspheres or that the BEC-tdT monolayer in the fluidic channel did not act as a sufficient barrier to the fibrin gel. In contrast, MVNs formed under flow conditions consistently achieved anastomosis, as demonstrated by microspheres flowing from high-pressure channels to the low-pressure channels through the open lumen of microvessels (Fig. 4B, Supp. Vid. 2). In flow culture, microspheres were rarely observed in the fibrin matrix surrounding microvessels. Due to the restrictive flow experienced by microspheres traveling through microvessels formed under static conditions, the mean microsphere velocity was 31.59 ± 8.72 μm/s. This was a stark contrast from the mean microsphere velocity of 521.77 ± 41.52 μm/s experienced by microspheres traveling through microvessels formed under flow conditions (Fig. 4C). Assuming that the velocity of the microspheres was the maximum velocity of the culture medium flowing through the microvessels, the fluid shear stress experienced by microvessels was estimated. These calculations gave a mean shear stress of 0.018 ± 0.006 and 0.394 ± 0.030 dyn/cm^2 for microvessels formed under static and flow conditions, respectively (Fig. 4D). Taken together, these data demonstrated that interstitial flow was necessary during MVN formation to develop microvessels capable of perfusion in this system. To reiterate, microvessels cultured under static conditions experienced neither luminal flow nor fluid shear stress leading up to the perfusion

experiment due to the lack of a hydrostatic pressure gradient. The calculated microsphere velocity and microvessel shear stress values were only possible due to the hydrostatic pressure difference (0.75 mmH_2O) created specifically for this perfusion experiment. Moreover, microvessels cultured under flow conditions were subjected to a higher hydrostatic pressure difference (1.5 mmH_2O) after each culture medium change. This resulted in luminal flow through every accessible microvessel until the reservoir volumes equilibrated. Although this did not last the full 24 hours between culture medium changes, we predicted that the flow experienced by microvessels would be significant enough to impact their morphology and function.

3.4 Interstitial flow enhanced brain microvascular network morphology and longevity

After it was observed that only MVNs cultured under flow conditions formed perfused microvessels, we hypothesized that the presence of interstitial and luminal flow would enhance microvessel formation. To measure this, BECs-tdT, PCs, and ACs were suspended in fibrin in the hydrogel channel and cultured under static or flow conditions for eight days. By Day 8, distinct brain MVNs had formed in both conditions (Fig. 5A). Microvessels were evaluated by several vascular parameters: vessel area, the number of vessel branches, average branch length and diameter, and the number of vessel segments. Comparing static to flow culture parameter means, vessel area increased from 38.19 ± 2.78 to 59.86 ± 1.79% (Fig. 5B), average branch length increased from 47.46 ± 2.16 to 58.68 ± 1.93 μm (Fig. 5D), and the average branch diameter increased from 28.65 ± 1.73 to 37.20 ± 1.36 μm (Fig. 5E), respectively. No statistical difference was found between the mean number of branches for MVNs formed under static (103.50 ± 5.19) and flow (102.00 ± 6.84) conditions (Fig. 5C). Lastly, the mean number of vessel segments (per area) was 2.83 ± 0.48 and 1.50 ± 0.22 for MVNs cultured under static and flow conditions, respectively (Fig. 5F). Collectively, these data indicate that the addition of interstitial flow increases the relative size of microvessels compared to those cultured without it. Once MVN anastomosis was achieved in the flow condition, microvessels became perfusable and experienced shear stress every time the hydrostatic pressure gradient was reset. As a result, vessel area, branch length, and branch diameter increased compared to that of microvessels cultured in static conditions. The increase in microvessel size increased the chance that neighboring vascular plexuses would amalgamate, reducing the amount of individual vessel segments. Indeed, MVNs cultured under flow conditions appeared more continuous than MVNs cultured under static

conditions, which still had individual microvessels separated from surrounding vessels on Day 8 (Fig. 5A). In summary, interstitial flow promotes the development of larger, more connected, microvessels when compared to microvessels cultured without flow.

After it was concluded that flow culture was beneficial for microvessel formation, we hypothesized that interstitial and luminal flow would prevent MVN regression during longer culture periods. To test this, BECs-EGFP, PCs, and ACs were cultured under static or flow conditions for 8 and 14 days. MVNs were observed in MFDs on Day 8 and Day 14 in samples cultured under both conditions (Fig. 5G). Visually, microvessels grown in flow culture on Day 8 and Day 14 were comparable and possessed wide, open lumen. In contrast, Day 14 microvessels grown in static culture were thinner than those on Day 8 and had narrower open lumen (Fig. 5G). To quantify these observations, three vascular parameters were selected to evaluate MVN maintenance over time: vessel area, average branch diameter, and the number of vessel segments. From Day 8 to Day 14, vessel area decreased from 45.76 ± 1.41 to 21.65 ± 2.65% (Fig. 5H), and average branch diameter decreased from 36.93 ± 2.36 to 20.91 ± 1.36 μm (Fig. 5I), respectively, for microvessels cultured in static conditions. In static culture, the number of vessel segments increased from 4.00 ± 0.86 to 9.33 ± 0.76 from Day 8 to Day 14, respectively (Fig. 5J). These values confirmed that MVNs in static culture decreased in size and became more fragmented from Day 8 to Day 14. In contrast, microvessels cultured under flow conditions saw no significant changes in vessel area (76.15 ± 2.29 to 70.65 ± 2.44%, Fig. 5H), average branch diameter (48.27 ± 1.64 to 45.98 ± 2.61 μm, Fig. 5I), and number of vessel segments (1.17 ± 0.17 to 1.33 ± 0.21, Fig. 5J) from Day 8 to Day 14, respectively. Plainly, MVNs formed in flow culture maintained their vascular characteristics for the duration of two weeks. The resulting difference between MVNs cultured under static and flow conditions can be attributed to the effect of interstitial and luminal flow on microvessels. Microvessels in static culture received no physical cues to maintain open lumen during extended culture. Contrastingly, after MVNs achieved anastomosis in flow culture, the microvessels were exposed to luminal flow daily. To reiterate, this provided the physical and biological cues for BECs to maintain mature, open lumen to compensate for the flow. Additionally, interstitial flow allows for more effective delivery of nutrients and removal of cellular waste products than simple diffusion. This was likely advantageous for cellular health and MVN maintenance in long-term culture. In summary, the presence of interstitial flow stymied microvessel regression and maintained MVNs longer than those cultured without interstitial flow.

3.5 Interstitial flow increased astrocyte coverage of microvessels

Next, we investigated if the presence of interstitial flow influenced PC and AC association with microvessels. To test this, BECs-tdT, PCs, and ACs were cultured under static or flow conditions for eight days. By Day 8, MVNs formed in both static and flow culture were comprised of tdTomato+ microvessels surrounded by NG-2+ PCs and GFAP+ ACs (Fig. 6A). Closer inspection revealed that both PCs and ACs were directly contacting hollow microvessels (Fig. 6B). PC and AC coverage was measured as a percentage of the total vessel area in the field of view. No statistical difference was found between the mean PC coverage of microvessels cultured under static (20.77 ± 1.99%) and flow (16.48 ± 1.13%) conditions (Fig. 6C). However, when comparing the mean AC coverage of microvessels in static and flow culture, an increase from 6.44 ± 0.71% to 9.20 ± 0.18% was observed, respectively (Fig. 6D). These data show that only AC coverage was enhanced under flow culture conditions.

Immunofluorescence images of MVNs revealed the presence of nuclei that did not possess any fluorescent marker (Fig. 6B). In 2D cell culture, we observed that PCs uniformly expressed NG-2 (Supp. Fig. 3A). While nearly all ACs were identified with GFAP in 2D cell culture, we observed a small population ACs with no visible GFAP signal (Supp. Fig. 3B). However, this was not surprising since AC expression of GFAP varies *in vivo*(52). When ACs transition to a reactive state, it is typically accompanied by an increase in cellular diameter, GFAP expression, and the number of astrocytic processes(52,53). For these reasons, we speculated that the unlabeled nuclei in MVNs could be those of ACs with no GFAP expression. We postulated that the increase in AC coverage of microvessels cultured under flow may be the result of an increase in the number of GFAP+ ACs or an increase in the amount of astrocytic process extensions in the fibrin gel. However, no statistical difference was found between the mean number of GFAP+ ACs (per area) observed in static (26.67 ± 1.74) and flow (28.83 ± 0.40) culture (Fig. 6E). Moreover, no statistical difference was found between the mean total length of AC processes (per area) observed in static (8.26 ± 0.64 mm) and flow (9.89 ± 0.46 mm) culture (Fig. 6F). Taken together, these data indicate that the slight increase AC coverage in flow culture is not due to a higher number of GFAP+ ACs or an increase in the total length of astrocytic processes.

3.6 Interstitial flow enhanced basal lamina protein production in microvessels

Endothelial protein expression is dependent on physical stimuli, such as shear stress(54). For this reason, we sought to determine if the presence of interstitial and luminal flow had an effect on microvessel protein production. To accomplish this, BECs-tdT, PCs, and ACs were cultured under static or flow conditions for eight days. On Day 8, immunofluorescence analysis was used to measure the expression of three proteins: ZO-1 (Fig. 7A), collagen IV (Fig. 7B), and laminin (Fig. 7C). All three proteins were observed in the MVNs cultured under both static and flow conditions. Previously, we stated that ZO-1 was observed to be localized at the borders of BECs (Fig. 3D). Basal lamina proteins, collagen IV and laminin, were observed along the border of microvessels (Fig. 7 B and C). To determine the relative expression levels of each protein, the total fluorescence intensity was normalized by the microvessel area. No significant difference was observed between the relative fluorescence intensity of ZO-1 of microvessels cultured under static (1.00 ± 0.05) and flow (0.88 ± 0.05) conditions (Fig. 7D). In contrast, we found that the presence of basement proteins was enhanced in flow conditions compared to static. When comparing relative static to flow means, collagen IV fluorescence intensity increased from 1.00 ± 0.03 to 1.85 ± 0.11, respectively (Fig. 7D). Similarly, when comparing relative static to flow means, laminin fluorescence intensity increased from 1.00 ± 0.07 to 1.84 ± 0.13, respectively (Fig. 7D). These data indicate that interstitial flow increases the amount of collagen IV and laminin located on microvessels, but not ZO-1, associated with BEC microvessels. In samples where ZO-1 and collagen IV were labeled simultaneously, similar trends were observed (Supp. Fig. 4). This confirmed that the increased pixel intensity of basement membrane proteins was not due to staining protocol errors. Taken together, these results suggest that interstitial flow has significant influence over the accumulation of basement membrane proteins on brain microvessels.

To confirm the presence of membrane transport proteins commonly found in the BBB, brain MVNs comprised of BECs-EGFP, PCs, and ACs were also cultured under static or flow conditions for eight days. On Day 8, both GLUT1 and P-gp were identified at the border of microvessels lumen in both culture conditions, indicating the expression of these membrane transporters in BECs-EGFP (Supp. Fig. 5). In addition, we observed nuclei in the interstitial space that were also co-labeled for GLUT1 and P-gp. These cells were not EGFP+ and therefore not BECs-EGFP. For this reason, we assumed that these nuclei belonged to either PCs or ACs, although we did not co-label these cells with NG-2 or GFAP, respectively. Due to the high

expression of GLUT-1 and P-gp in all brain MVN cell types, we did not perform any immunofluorescence analysis on these membrane transport proteins as it would be difficult to distinguish proteins exclusively expressed by microvessels.

Based on the idea of flow-mediated protein expression, we tested if the presence of interstitial flow had an effect on MVN protein secretion. We selected BDNF, a prominent neurotrophin, as the target protein for ELISA. In the mammalian brain, BDNF is predominantly produced and secreted by BECs(55,56) but has also been reported to be derived from PCs(57) and ACs(58), albeit at lower quantities. We cultured BECs, PCs, and ACs under static or flow conditions and collected the conditioned culture medium to test for the presence of BDNF on Days 2, 4, and 6. We considered higher concentrations of BDNF to be present in conditioned medium from flow samples simply due to interstitial flow removing soluble BDNF from the fibrin gel. However, we believed that this factor would be negligible due to the equilibration of the hydrostatic pressure difference in flow culture. We previously reported that the interstitial flow rate after 9 hours was essentially negligible (Results 3.1). Therefore, the distribution of soluble BDNF for the remaining 15 hours between volume reestablishment would be dependent on diffusion and identical to static conditions. After 15 hours without interstitial flow, we assumed that the concentration of BDNF reached an equilibrium throughout the fluidic channels of flow samples. This, coupled with the collection of conditioned culture medium every 48 hours from both high-pressure and low-pressure reservoirs, reduced the possibility that higher concentrations of BDNF in flow culture would be solely the result of convective mass transfer. The concentration of BDNF in conditioned culture medium from Day 2 was below the minimum detectable limit of the ELISA kit (data not shown). However, BDNF concentration was able to be measured for culture medium collected from Day 4 and Day 6 (Supp. Fig. 6B). Between Day 4 and Day 6, the concentration of soluble BDNF increased from 25.29 ± 6.94 to 71.42 ± 21.96 pg/mL, respectively, in static culture. Similarly, in flow culture, the BDNF concentration increased from 49.41 ± 11.65 to 112.79 ± 17.26 pg/mL from Day 4 to Day 6, respectively. These results show that the mean BDNF concentration was measured to be higher in flow culture than static culture on Day 4 and Day 6, however, no significant difference was calculated. From these data, we concluded that the presence of interstitial flow did not enhance the concentration of soluble BDNF in MFDs.

3.7 Interstitial flow decreased microvessel permeability

Lastly, we tested if the presence of interstitial flow had an influence on microvessel barrier function. To determine this, BECs-EGFP, PCs, and ACs were cultured under static or flow conditions for eight days. On Day 8, microvessels from all samples were perfused with 70 kDa dextran solution to measure the rate at which dextran permeated into the surrounding fibrin ECM (Fig. 8A). As demonstrated in the microsphere perfusion experiment, only MVNs cultured under flow conditions achieved anastomosis and experienced luminal flow (Fig. 4A and B). Similarly, in preliminary experiments, we observed that only microvessels cultured under flow conditions were able to be perfused with Oregon Green dextran (70 kDa) solution (Supp. Fig. 7). In MVNs cultured under static conditions, most microvessel segments located in the hydrogel channel were inaccessible to the dextran solution. Eventually, dextran diffused into the center of the hydrogel channel and revealed the outline of hollow, non-perfused microvessels grown in static culture (Supp. Fig. 7). For these reasons, time-lapse confocal images of microvessels grown in static and flow culture were acquired near the gel-liquid interface and the center of the hydrogel channel, respectively. For MVNs cultured under static conditions, dextran solution entered microvessels at the hydrogel-liquid interface and was initially retained in the vascular lumen (Fig. 8A). After 150 seconds, trace amounts of dextran visibly leaked into the surrounding fibrin matrix. For MVNs cultured under flow conditions, dextran perfused into mature microvessels and was observed predominantly in the vascular lumen for the duration of imaging (Fig. 8A). The dextran permeability coefficient for microvessels cultured under static and flow conditions was found to be $8.07 \pm 0.90 \times 10^{-7}$ and $2.35 \pm 0.27 \times 10^{-7}$ cm/s, respectively (Fig. 8B). These results indicate that microvessels cultured under static conditions are more permeable to dextran than those cultured under flow conditions. Indeed, the maximum permeability coefficient for microvessels in static culture (1.16×10^{-6} cm/s) was nearly a full order of magnitude higher than the maximum value in flow culture (3.23×10^{-7} cm/s). In addition, the permeability coefficient values calculated for static culture were observed over a larger range than the values calculated for flow culture. Taken together, these data indicate that culturing MVNs under flow conditions enhances microvessel barrier function.

4. Discussion

In this work, we successfully developed 3D brain MVNs within a MFD and demonstrated the importance of interstitial flow regarding their formation, maintenance, and function. The MFD used from AIM Biotech has been implemented in previous studies, highlighting its utility and potential for adoption by other laboratories(50,59,60). Our microfluidic model included self-assembled human MVNs comprised of primary BEC microvessels supported by PCs and ACs, mimicking capillary networks found in the brain(2,4). Brain MVNs were formed through natural endothelial processes and did not rely on physiologically-inaccurate channel geometries and configurations, like several previous MFD models(13,61–64). The benefits of interstitial flow on vasculogenesis and angiogenesis have previously been characterized using non-brain endothelial cells(39,40,65). However, in these studies, a majority of microvessel analysis was focused on morphological changes in response to interstitial flow. We present the first microfluidic model to characterize multiple effects of interstitial flow on brain-specific microvessel formation in the presence of PCs and ACs. Campisi and colleagues recently reported the development of similar brain MVNs using human induced pluripotent stem cell-derived endothelial cells in the absence of interstitial flow(16). Despite the resemblance to this experimental setup, we were unable to generate perfused microvessels in our model under static conditions. This distinction emphasizes how different experimental variables can drastically alter the functionality of brain MVNs developed *in vitro*. To produce perfused brain microvessels, we generated interstitial flow in our model and observed marked differences in vascular parameters as a result. Due to the dramatic effect on microvessel morphology, we continued our investigation to further elucidate the influence of interstitial flow on other characteristics of brain microvasculature. Recently, Figarol and colleagues studied the effects of continuous interstitial flow on brain MVNs using a Transwell-based model(47). When compared to that study, our present work possesses three major distinctions: 1) Formation of 3D brain MVNs within a MFD; 2) Development of microvessels with open lumen capable of perfusion; and 3) Quantitative analysis of multiple vascular morphological features, luminal flow and shear stress, PC and AC coverage, soluble protein concentration, and microvessel barrier function. These analyses demonstrate our model's potential to study the biological relevance of the bulk flow of interstitial fluid on the formation of functional human brain MVNs.

To study the effect of interstitial flow on human brain MVN formation, two experimental conditions were created in the MFD: static and flow. In static conditions, a pressure difference of 0 mmH_2O generated an average dextran solution flow velocity of 0.08 μm/s (Fig. 1D) and volumetric flow rate of 0.22 nL/s (Fig. 1E) across the fibrin gel. Obviously, a pressure difference of 0 mmH_2O physically should not have generated any convective flow. The minuscule velocity and flow rate measured can likely be attributed to minute height differences in reservoir volumes due to pipetting error and unlevel imaging surfaces. Therefore, for all samples cultured under static conditions, the movement of solutes in the fibrin hydrogel was assumed to be completely dependent on diffusion. In flow conditions, a pressure difference of 1.5 mmH_2O generated an average dextran solution flow velocity of 5.73 μm/s (Fig. 1D) and volumetric flow rate of 15.03 nL/s (Fig. 1E) across the fibrin gel. These data represented the maximum values obtained in the flow condition and confirmed that the movement of solutes through the fibrin hydrogel was initially governed by convection. Simulated data showed that interstitial flow velocity and rate decayed until they reached values three orders of magnitude lower after approximately 9 hours (Fig. 1F and G). During that time period, the bulk flow experienced by the fibrin gel was within the physiological range of interstitial flow found in most soft tissues (0.1 to 10 μm/s)(22,35,66,67). This feature of our model is critical considering the regulatory role of interstitial fluid flow in communication between neural, glial, and vascular cell types(36).

Although flow samples experienced nonzero convective flow rates after 9 hours, they were in the order of picoliters per second and therefore considered insignificant. Our experimental design's largest shortcoming was the lack of continuous flow after the reservoir volume equilibration. Cells in flow culture experienced conditions similar to static culture for extended time periods (approximately 15 hours) between medium changes. We also acknowledge that interstitial flow rates through cell-laden fibrin gels may differ from those through empty gels used to determine fibrin hydrogel permeability. However, our equation used to calculate hydrogel permeability (Eq. S2) does not contain a variable to account for the presence of dispersed objects, such as cells. With that said, the purpose of that experiment was to highlight the stark difference between the movement of fluid through fibrin gels in static and flow conditions and obtain an estimate of the interstitial flow rate over time. In actuality, the interstitial flow rate profile likely changed as BECs expanded and fused into microvessels in the hydrogel channel. Additionally, the BEC monolayer seeded in both fluidic channels (Fig. 3C) on Day 3 likely acted as a physical

barrier to flow across the length of the fluidic channel. This barrier would have decreased the interstitial flow rate and extended the time before equilibrium was reached. However, the equations used to simulate bulk flow through the fibrin hydrogel over time do not consider the presence of a semi-permeable barrier and could not be used to simulate interstitial flow after Day 3 (Supplementary Methods S.1). Moreover, the pressure difference certainly decreased at a faster rate once MVN anastomosis was achieved. Although luminal flow is a desired attribute of brain capillaries, limited reservoir volumes prevented long-term exposure to this stimulus. These problems could be circumvented by the implementation of a microfluidic pump that constantly maintained the pressure across the hydrogel channel(68). However, we used a pumpless microfluidic system because it was simpler, cheaper, occupied less space, and used low reagent volumes. Future experiments with pumpless MFDs could implement larger reservoir attachments or ECMs with lower permeabilities to extend flow culture periods. Despite the limitations of our design, we chose to implement non-continuous interstitial flow in our cultures because it was substantial enough to produce a quantifiable effect on brain MVN formation and function.

To the best of our knowledge, we are the first group to use a MFD to explore the effects of interstitial flow on BEC angiogenesis in the presence of PCs and ACs. BEC angiogenesis was enhanced under flow conditions, as evidenced by the increase in sprout number, length, and diameter observed by Day 7. In addition to the inclusion of VEGF in the culture medium, PCs and ACs were seeded within the fibrin hydrogel to encourage angiogenic sprouting, similar to Lee and colleagues(17). We predicted that PCs and ACs would promote endothelial morphogenesis through direct cell-cell contact and the secretion of pro-angiogenic factors(2,4,69,70). However, in our study, BEC angiogenesis was mediated by both biological and physical cues. In flow culture, we observed enhanced angiogenesis against the direction of interstitial flow (Fig. 2B), similar to previous studies using non-brain endothelial cells(22,71). Those studies reported that interstitial flow attenuated soluble factor gradients and acted as the directional cue for angiogenesis(22,71). In our design, the mean interstitial flow rate experienced by BEC angiogenic sprouts at the inception of flow culture was 5.73 μm/s. This value is close to the interstitial flow rate used in previous studies (6 μm/s) to eliminate any established morphogen gradient in MFDs(22,65,72). Although our flow rate decreased exponentially over time, the direction of bulk fluid movement remained the same until reservoir volume equilibration. Until that moment, it is likely that no gradients of soluble growth factors released by PCs and ACs were able to develop due to the

presence of interstitial flow through the fibrin gel. The evident difference between the morphology of angiogenic sprouts in static and flow culture highlights the necessity of implementing interstitial flow in future *in vitro* models of brain microvessel sprouts.

We observed the formation of brain MVNs in both static and flow cultures. However, microsphere perfusion demonstrated that microvessels formed under static conditions did not allow for significant luminal flow. In contrast, most microvessels grown in flow culture possessed perfused lumen. Although we predicted that flow conditions would increase the chance of microvessel perfusion, we did not anticipate the complete lack of anastomosis in static samples. Previous studies have shown that brain MVNs generated without interstitial flow were able to be perfused with dextran solutions(16,17). This distinction from our observations highlights the potential impact of experimental design variables (cell source, density, arrangement, and ECM composition) on the generation of perfused microvessels. Our study showcases that the addition of interstitial flow is sufficient enough to achieve anastomosis uniformly and reproducibly in cell-laden hydrogels that would otherwise be non-perfused. Although interstitial flow has been shown to promote the anastomosis of capillary networks comprised of non-brain endothelial cells(22–26,40,41), we are the first to report the direct influence of interstitial flow on the perfusion of brain MVNs developed within a MFD. Future researchers should consider the application of interstitial fluid flow in their models to increase the chance of developing perfused microvessels.

With a pressure of 0.75 mmH_2O, the average microvessel shear stress experienced by MVNs formed in static and flow conditions was 0.018 and 0.394 dyn/cm^2, respectively (Fig. 4D). Although shear stress values vary depending on the vessel, the shear stress experienced by microvessels in flow culture was within the range of reported physiological values (0.1-60 dyn/cm^2)(73,74). It can be assumed that microvessels in flow culture experienced wall shear stress values comparable to those observed in certain brain microvessels. However, the shear stress experienced during microsphere perfusion by microvessels from static culture resembled that of extremely low flows present during early blood vessel formation ($\sim 10^{-2}$-10^{-4} dyn/cm^2)(74). To reiterate, these values were only experienced by microvessels briefly during the perfusion assay. Microvessels in static conditions did not experience significant shear stress during culture. As a further point, microvessels grown under flow conditions likely experienced higher shear stress values when a pressure difference of 1.5 mmH_2O was applied. Vessel wall shear stress is paramount for vascular health and is directly responsible for cytoskeletal remodeling,

transcriptional regulation of genes, and activation of signaling cascades in endothelial cells(73,75). A critical design flaw in previous microfluidic models of MVNs is the lack of luminal flow present during microvessel development(16,49,51,76). Although our experimental design did not have continuous flow, we predicted that intermittent luminal flow would have significant effects on microvessel formation and function.

To the best of our knowledge, we are the first to explore the effects of interstitial flow on brain MVN formation within a MFD. After 8 days, the average branch diameters (Fig. 5E) of microvessels in static (28.65 μm) and flow (37.20 μm) were within the range for that of brain microvasculature observed *in vivo* (3 to 100 μm)(18,19). MVNs cultured under flow conditions produced larger, more connected microvessels than those cultured under static conditions. This was probably due to the higher availability of nutrients and the more efficient removal of cellular waste due to convective fluid transport through the fibrin hydrogel. However, the principal reason for this discrepancy in microvessel morphology was likely the result of luminal flow experienced after MVN anastomosis. Wall shear stress and transmural pressure gradients regulate blood vessel diameter, depending on the elasticity and thickness of the vascular wall(73,77). The luminal flow experienced by microvessels in flow conditions plausibly caused microvessels to grow in diameter, as well as maintain their morphology for extended culture. Shear stress-induced vessel dilation has been shown to be accompanied by enhanced endothelial cell nitric oxide production, cytoskeletal reorganization, and increased ECM interaction through integrins(78,79). In addition, microvessel enlargement due to perfusion likely promoted the fusion of adjacent expanding vessels, creating interconnected MVNs. Microvessel fusion in static culture was dependent solely on paracrine signaling from proximal cells and local ECM remodeling. The discernible effect of interstitial flow on microvessel morphology adds credence to the importance of implementing bulk interstitial fluid flow when generating brain MVNs *in vitro*.

We did not observe significant changes in vascular morphology in microvessels cultured under flow conditions between Day 8 and 14. In contrast, microvessels in static culture decreased in size and were more segmented after two weeks. Interstitial and luminal flow likely prevented significant microvessel regression through shear stress-mediated processes previously described(78,79). Blood vessel regression and pruning is a natural part of vascular remodeling(80). However, the fragmented microvessels observed in static culture on Day 14 were likely the result of vessel destabilization induced by the lack of physical and biological stimuli. Previous studies

of brain MVNs developed *in vitro* were typically terminated after approximately one week in culture(16,17). It is possible that microvessels developed in these MFDs would regress in long-term culture due to the absence of interstitial and luminal flow. In our model, the presence of microvessels with open lumen after two weeks of flow culture confirms the importance of interstitial flow for vessel maintenance as well as highlights the potential longevity of this experimental design. The maintenance of perfused brain MVNs is advantageous for *in vitro* models attempting to recapitulate time-intensive biological processes of the neurovascular unit, such as neurogenesis or neurodegenerative disease progression(81,82). The optical transparency of this MFD also facilitates the long-term visualization of these cellular interactions, which would be difficult to perform in *in vivo* models.

The MVNs developed in static and flow culture were comprised of BEC microvessels supported by PCs and ACs (Fig. 6B). Both PCs and ACs are fundamental for vascular health and regulate BBB function(2,4). In our model, PCs associated with microvessels directly while ACs extended processes which terminated in endfeet at the microvessel border. It was postulated that PCs and ACs would secrete pro-vasculogenic factors and promote microvessel maturation through direct contact with BECs(16). We initially hypothesized that the presence of interstitial flow would increase PC and AC microvessel coverage. However, only AC coverage was enhanced for microvessels cultured under flow conditions compared to static culture. This was not the result of an increase in the number of GFAP+ ACs or the total length of astrocytic processes in the fibrin gel. Microvessels likely came into contact with proximal astrocytic processes as they dilated. The lumen of microvessels formed in static conditions did not expand as extensively as those in flow conditions. Therefore, we surmised that the enhanced AC coverage was likely due to the physical expansion of microvessels and not a direct response of astrocytes to interstitial flow. It is also possible that microvessels in flow conditions produced soluble signals that better attracted astrocytic endfeet, however we did not investigate this. Nonetheless, increased AC coverage may be useful in future studies to investigate the interactions of vascular and glial cells. As an example, the clearance of harmful proteins from the brain through the glymphatic system is dependent on the function of perivascular channels dictated by aquaporin-4 on astroglial endfeet(37). The study of this macroscopic waste removal *in vitro* would be applicable for characterizing the progression of human neurodegenerative diseases(83).

The presence of interstitial flow was the independent variable in our experiments. However, once anastomosis was achieved in flow culture, microvessels were likely influenced by intraluminal flow as well. Indeed, shear stress from luminal flow in blood vessels has a direct effect on the gene expression of vascular endothelial cells(44,75,84). We hypothesized that shear stress experienced by microvessels from luminal flow would enhance the expression of BBB-related proteins in BECs. While there was no change in the relative fluorescence intensity of ZO-1, an increase in collagen IV and laminin intensities was observed in microvessels cultured in flow conditions compared to static (Fig. 7D). We found this result interesting considering that previous studies have demonstrated that laminar shear stress enhances the expression of several endothelial cell tight junction proteins, including ZO-1(46,85). However, no difference in the expression and localization of claudin-5, occludin, and ZO-1 was observed for iPSC-derived human brain microvascular endothelial cells subjected to shear stress(86). Furthermore, while Figarol and colleagues observed an upward trend in protein and gene expression of claudin-5 and ZO-1 in brain microvascular endothelial cells exposed to interstitial flow, no significance was reported(47). Due to these results, as well as our own ZO-1 data, we did not test the expression of other tight junction associated proteins. It is possible that the intermittent shear stress profile BECs experienced during flow conditions was not conducive to tight junction improvement. Nonetheless, the enhanced fluorescence intensity of collagen IV and laminin under flow conditions correlated with data from previous studies. Endothelial cells exposed to high shear stress saw a significant increase in the mRNA expression of collagen IV compared to those in static conditions(87). In addition, endothelial cells experiencing shear stress were reported to have reduced production and secretion of matrix metalloproteinase-2 (MMP2), which degrades basement membrane proteins such as collagen IV(87,88). Basement membrane remodeling of laminin structures and laminin-associated integrins was also observed in endothelial cells exposed to flow-induced shear stress(89). Lastly, laminin 511 was previously identified as an endothelial cell-derived basement membrane protein that was essential for shear stress response(90). Taken together, these results conclude that shear stress upregulates basal lamina proteins that are responsible for vascular remodeling as well as shear stress detection. For these reasons, we surmise that the shear stress experienced by microvessels in flow culture was the cause of the enhanced fluorescence intensity observed for collagen IV and laminin. It is possible that interstitial flow experienced on the basolateral membrane of microvessels contributed to increased basement

membrane production. However, we found no literature that claimed that interstitial fluid flow specifically influenced collagen IV and laminin production. Moreover, the increased mean intensities of collagen IV and laminin experienced in flow culture do not necessarily indicate that basement membrane protein production was enhanced. It is possible that basement membrane degradation was reduced in flow culture, compared to static, which would align with previous studies regarding endothelial cell MMP production(87,88). Future studies regarding mRNA levels, as well as the concentration of extracellular MMPs, are needed to confirm the cause of the increased intensity of basement membrane proteins.

We confirmed the expression of both GLUT1 and P-gp in microvessels comprised of BECs-EGFP cultured under static and flow conditions (Supp. Fig. 5). The localization of GLUT1 and P-gp on BECs is critical for the function of the BBB *in vivo*(1). The expression of both membrane transport proteins in BECs-EGFP indicates the presence of a microvessel transport barrier. However, we also observed the expression of GLUT1 and P-gp in all cells not expressing EGFP, which were assumed to be PCs and ACs by default. Although we predicted that these membrane transporters would be localized exclusively at the luminal and abluminal membrane of BECs, the expression of GLUT1 and P-gp is not uncommon in mural and glial cells. Indeed, in addition to BECs, GLUT1 has been shown to be expressed in vascular pericytes(91–93) and astrocytes(94,95). Similarly, P-gp has been reported to be localized along brain capillaries as well as adjacent pericytes(96,97) and astrocytes(96,98,99). The presence of GLUT1 and P-gp in the membranes of BECs, PCs, and ACs suggests that these proteins govern the transportation of substrates throughout the entire brain at the cellular level(1). The expression of both transmembrane proteins in all brain MVN cell types in our model give credence to its ability to potentially replicate this substrate regulation *in vitro*. Moreover, P-gp has a significant role in modulating multidrug resistance of numerous brain tumors(100). An *in vitro* model of human brain MVNs with physiologically-accurate expression and localization of P-gp would be valuable for the development of effective anti-cancer drugs.

We further speculated that flow conditions would enhance BEC secretion of BDNF since endothelial cells have been shown to exhibit flow-specific protein secretion patterns(101). However, flow culture did not significantly increase BDNF concentration compared to static culture, indicating that interstitial flow had no discernable effect on the secretion of BDNF. It is possible that a statistical difference would have been found with a larger sample size. Due to the

absence of interstitial flow for the majority of time (approximately 15 hours) between reservoir volume height reestablishment in flow samples, we maintain that the concentration of soluble BDNF was predominantly due to cellular secretion and not the removal of BDNF from the fibrin gel due to bulk fluid movement. Nonetheless, the increase in BDNF concentration between Day 4 and Day 6 in both static and flow conditions demonstrated that MVN cells (predominantly BECs) increased their secretion of the neurotrophin as microvessels matured. This is encouraging for generating *in vitro* models of brain MVNs to recapitulate the neurovascular unit, given the critical role of BDNF in neuron survival and maturation.

Healthy brain capillaries are characterized by low permeability to most molecules, including dextran(1). Dextran (70 kDa) permeability coefficients of 8.07×10^{-7} and 2.35×10^{-7} cm/s were calculated for microvessels cultured under static and flow conditions, respectively (Fig. 8B). In our model, microvessels cultured under both conditions had lower permeabilities compared to other human *in vitro* BBB models that implemented Transwells(102–104) or endothelial cell-lined microfluidic channels(13,61). This demonstrated an advantage of MVNs being formed through natural morphogenic processes *in vitro*. However, only the mean permeability coefficient for microvessels in flow culture was comparable to that of rat cerebral microvessels (1.5×10^{-7} cm/s)(105) and human MVNs formed in MFDs(49,106). Microvessels formed under static conditions were visibly leakier than those formed under flow conditions. Initially, we considered conducting permeability studies with alternative molecules (Lucifer yellow and rhodamine 123). However, the stark contrast between the average dextran permeability of static and flow samples effectively demonstrated the improvement in barrier function due to interstitial flow. It is unlikely that the opposite trend would be observed with solutes of lower molecular weights. Although we hypothesized that interstitial flow would reduce permeability to dextran, we found our results interesting considering the localization of ZO-1 at BEC junctions observed on microvessels grown in static and flow culture (Fig. 3D). In addition, no difference in ZO-1 fluorescence intensity was recorded between microvessels from both conditions (Fig. 7D). Given the role of ZO-1 in the function of the BBB(107), we expected the difference in microvessel permeability values between static and flow cultures to be less pronounced. However, microsphere perfusion revealed that static conditions produced microvessels that allowed microspheres to leak into the fibrin extracellular space (Fig. 4B). Given the much smaller size of a dextran molecule to a microsphere, it is not surprising that dextran was able to permeate into the fibrin matrix, despite the presence of healthy

tight junction proteins. This might also explain the larger range of permeability values observed in static samples, as less porous microvessels might possess barrier functions comparable to those of microvessels grown in flow culture. Moreover, basal lamina proteins, such as collagen IV and laminin, act as a physical barrier that contribute to low permeability of brain capillaries(108). It is possible that the increased accumulation of basement membrane proteins in the perivascular space of microvessels in flow culture contributed to their vascular function. Lastly, since ACs provide cellular signals that enhance endothelial cell barrier function, it is also possible that the increased AC coverage of microvessels observed in flow culture had an effect on vascular permeability, although we did not investigate this(4). In conclusion, the generation of perfusable, semi-permeable microvessels under flow conditions emphasizes the importance of interstitial flow in the formation of functional brain MVNs. This is significant to the development of future *in vitro* BBB models and validates the use of this design for future drug screening and permeability studies(109).

5. Conclusion

In this study, we have demonstrated the significance of interstitial flow in the development of human brain MVNs within a MFD. MVNs possessed the proper cellular interactions from PCs and ACs and expressed BBB-related proteins. Under flow conditions, microvessels were perfused and exhibited improved vascular morphological features as well as enhanced endothelial barrier function. These results demonstrated the notable influence of interstitial flow on brain MVN formation and highlighted the coupling of physical and biological cues that regulate brain microvessel maturation. Together, these features make our experimental design an ideal *in vitro* model of human brain microvasculature that can be easily replicated by other laboratories. The presence of perfused, functional brain MVNs will be valuable in preclinical studies to determine the efficacy of drugs for the central nervous system that rely on vascular delivery(109). Moreover, modification of the current experimental design could be used to study the progression of neurodegenerative diseases that are characterized by BBB dysfunction(5–10). Lastly, future mechanistic studies can be performed in this platform to elucidate the cellular mechanics of interstitial flow-mediated microvessel function.

Author Contributions

Max Winkelman is the primary author and was responsible for all research investigation, analysis, and visualization, as well as the writing of the published work. Diana Kim is a co-author and was responsible for assisting in the investigation of vasculogenesis experiments. Shravani Kakarla, Nathaniel Silvia, and Alexander Grath are co-authors and were responsible for assisting in the investigation of longevity experiments. Diana Kim, Shravani Kakarla, and Nathaniel Silvia were also responsible for the review and editing of the manuscript in pre-publication stages. Guohao Dai is the principal investigator for this project, as well as the corresponding author for this publication.

Conflicts of Interest

There are no conflicts of interest to declare.

Acknowledgments

We thank the support from the National Institutes of Health Grants R01NS107462, R21NS121736, National Science Foundation CBET-1350240, American Heart Association 19IPLOI34760604. We also thank the Institute for Chemical Imaging of Living Systems at Northeastern University for the use of confocal microscopes and software. Lastly, we acknowledge BioRender.com for the generation of the graphical abstract illustration.

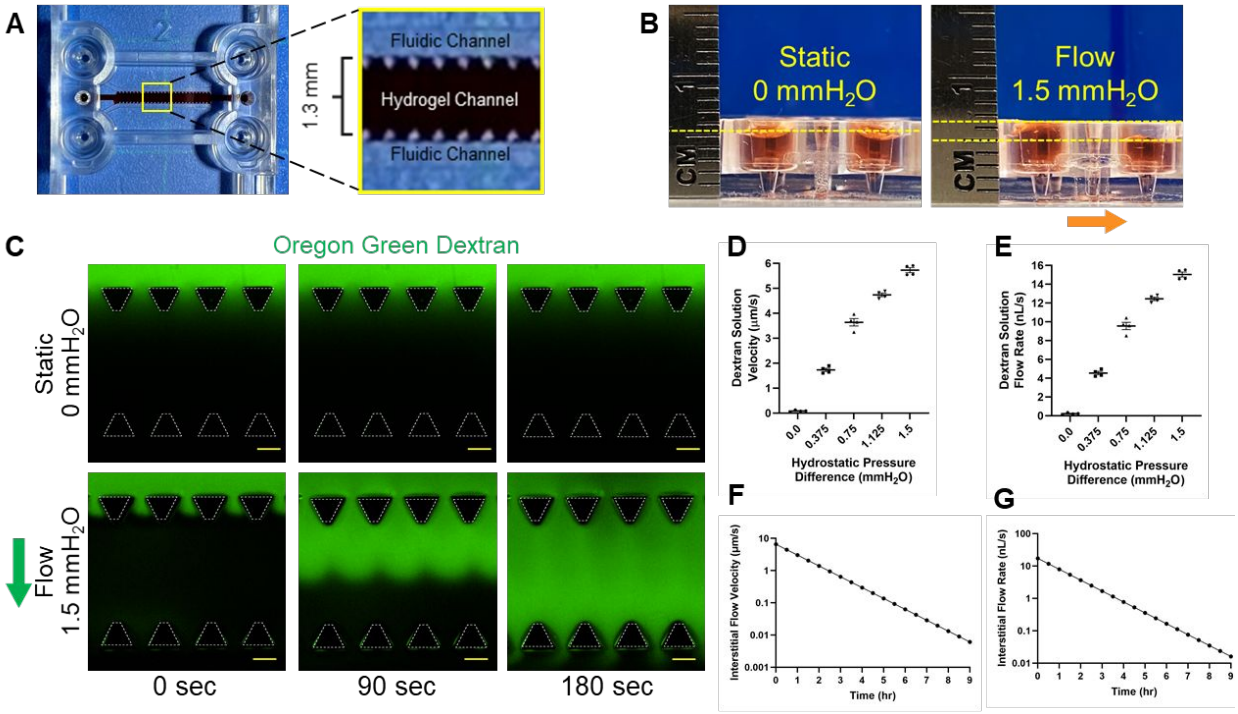

Figure 1. Interstitial flow characterization in MFD. A) Image of MFD from AIM Biotech (Singapore). Second image shows enhanced view of yellow square. B) Images showing the sideview of reservoir volumes used for static and flow culture. For static and flow conditions, culture medium was added to produce a hydrostatic pressure difference of 0 and 1.5 mmH_2O, respectively. Orange arrow indicates direction of interstitial flow of culture medium across the hydrogel channel. Yellow dashed lines identify reservoir volume heights. C) Fluorescence time-lapse images of Oregon Green 70kDa dextran solution (green) flowing through cell-free fibrin gels under static and flow conditions at 0, 90, and 180 seconds. Green arrow indicates direction of flow of dextran solution. White dashed lines outline microposts. Scale bars indicate 200 μm. D, E) Graph of dextran solution velocity (D) and flow rate (E) measured at pressure differences from 0 to 1.5 mmH_2O. The data show mean value, error bars ± SEM, n = 4. F, G) Graph of simulated interstitial flow velocity (F) and flow rate (G) experienced over 9 hours during flow (1.5 mmH_2O) conditions.

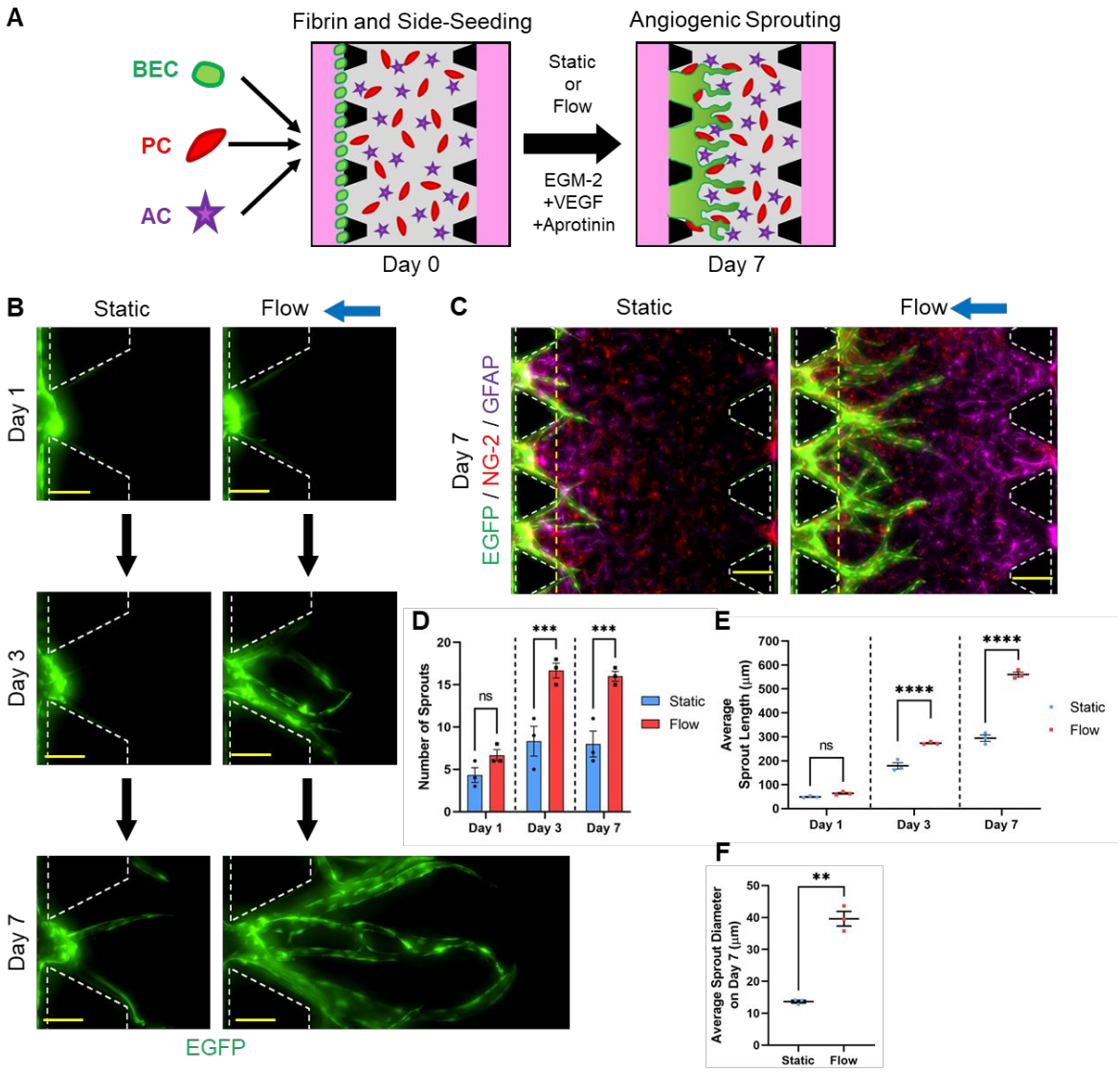

Figure 2. BEC angiogenesis in MFD. A) Illustration of the protocol to study BEC angiogenesis. On Day 0, PCs (red) and ACs (purple) were suspended in a fibrin matrix in the hydrogel channel and BECs (green) were side-seeded at the hydrogel-liquid interface of one fluidic channel. Cells were cultured in EGM-2 (+VEGF, +Aprotinin) under static or flow conditions for one week. B) Fluorescence images of BECs (EGFP, green) extending angiogenic sprouts into the fibrin hydrogel under static and flow conditions on Day 1, 3, and 7. PCs and ACs were not labeled. Scale bars indicate 100 μm. C) Fluorescence images of BEC (EGFP, green) angiogenic sprouts supported by PCs (NG-2, red) and ACs (GFAP, purple) grown under static and flow conditions on Day 7. Yellow dashed lines indicate distance at which the sprout diameter was measured. Scale bars indicate 200 μm. B, C) Blue arrows indicate direction of interstitial flow. White dashed lines outline microposts. D, E) Graph of the number of sprouts (D) and the average sprout length (E) observed for BECs-EGFP with PCs and ACs under static and flow conditions on Day 1, 3, and 7. F) Graph of the average sprout diameter observed for BECs-EGFP with PCs and ACs under static and flow conditions on Day 7. D-F) The data show mean value, error bars ± SEM, n = 3, ns $p > 0.05$, ** $p < 0.01$, *** $p < 0.001$, **** $p < 0.0001$.

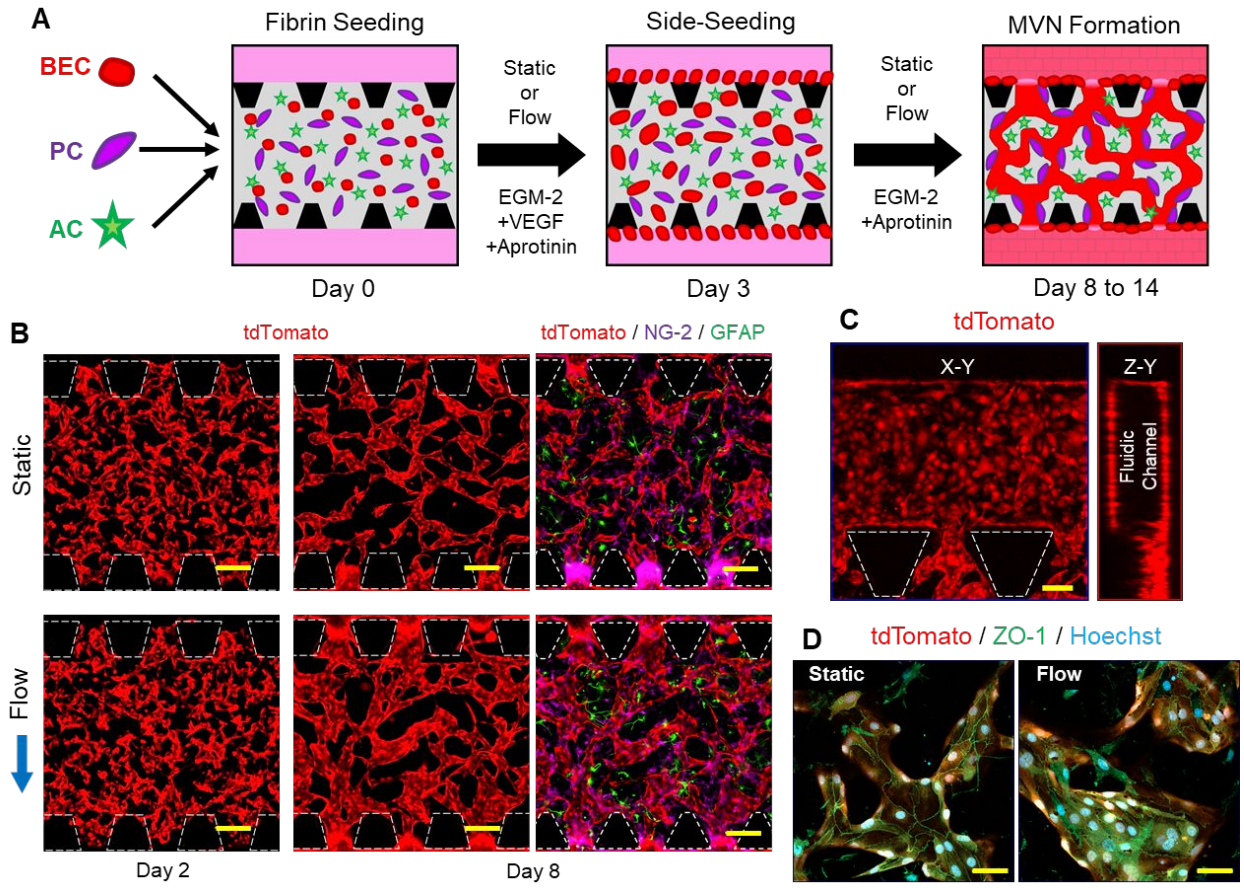

Figure 3. Brain MVN formation in MFD. A) Illustration of the protocol to study BEC vasculogenesis. On Day 0, BECs (red), PCs (purple), and ACs (green) were suspended in a fibrin matrix in the hydrogel channel. Cells were cultured in EGM-2 (+VEGF, +Aprotinin) under static or flow conditions for three days. On Day 3, BECs were side-seeded in both fluidic channels. Cells were then cultured in EGM-2 (+Aprotinin) under static or flow conditions until either Day 8 or 14. B) Fluorescence images of BECs (tdTomato, red) forming MVNs under static and flow conditions on Day 2 and 8. PCs and ACs were labeled with NG-2 (purple) and GFAP (green), respectively, on Day 8. Blue arrow indicates direction of interstitial flow induced during flow condition. Scale bars indicate 200 μm. C) Maximum intensity projection of fluorescence confocal image of BECs (tdTomato, red) side-seeded in the fluidic channel on Day 8. Image shows the cross-sectional view of the X-Y and Z-Y planes. B, C) White dashed lines outline microposts. D) Confocal fluorescence images BECs (tdTomato, red) expressing ZO-1 (green) under static and flow conditions on Day 8. C, D) Scale bars indicate 50 μm.

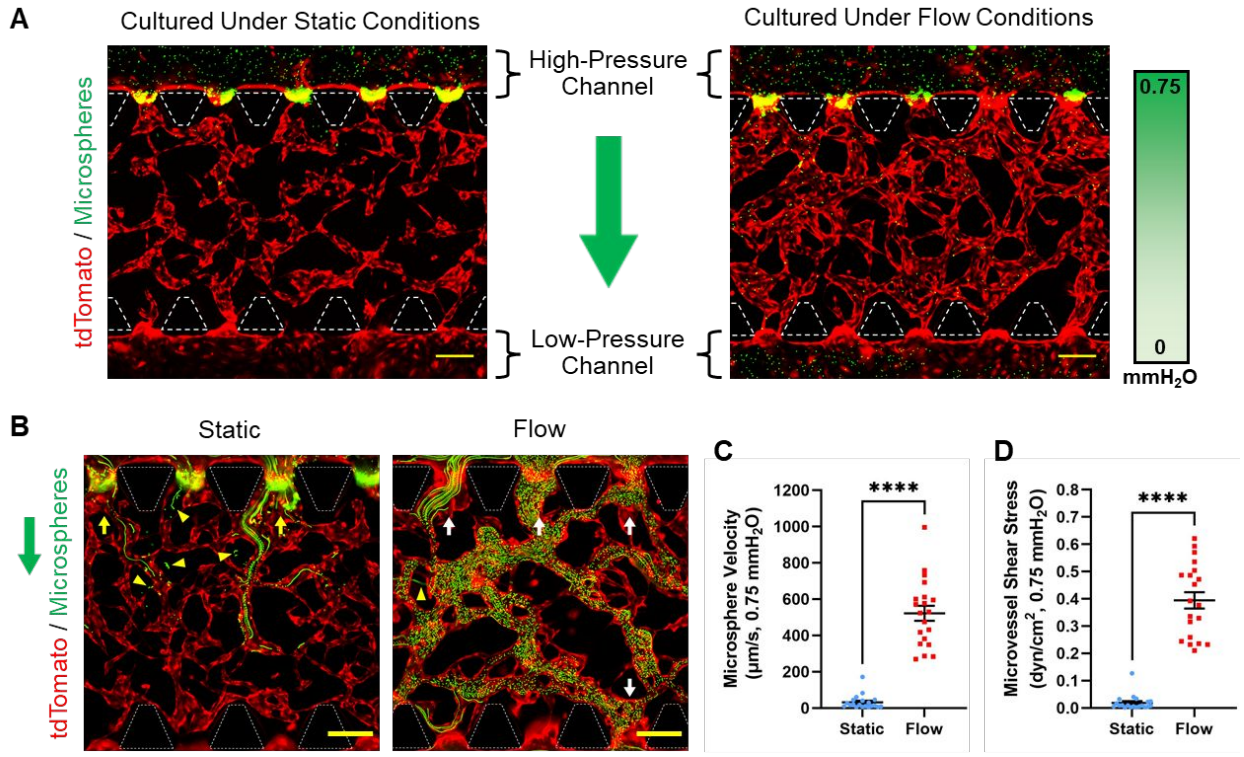

Figure 4. Microsphere perfusion assay. A) Fluorescence images of microsphere (green) perfusion experiment for microvessels (tdTomato, red) cultured under static and flow conditions. Culture medium with and without microspheres was added to the high-pressure and low-pressure fluidic channels, respectively, to create a hydrostatic pressure difference of 0.75 mmH_2O. B) Maximum intensity projection of fluorescence time-lapse images (30 seconds) of microspheres (green) flowing through microvessels (tdTomato, red) formed under static and flow conditions. White and yellow arrows indicate open lumen with and without egress for microspheres, respectively. Yellow triangles point to microspheres that have leaked into the fibrin gel. Original time-lapse videos for static and flow sample are presented as Supp. Vid. 1 and 2, respectively. A, B) Green arrows indicate direction of microsphere solution flow during perfusion experiment. White dashed lines outline microposts. Scale bars indicate 200 μm. C, D) Graph of microsphere velocity (C) and microvessel shear stress (D) experienced by MVNs formed under static and flow conditions with a pressure difference of 0.75 mmH_2O. The data show mean value, error bars ± SEM, microsphere velocity and microvessel shear stress values (n = 20) were measured from one sample per culture condition, ****$p < 0.0001$.

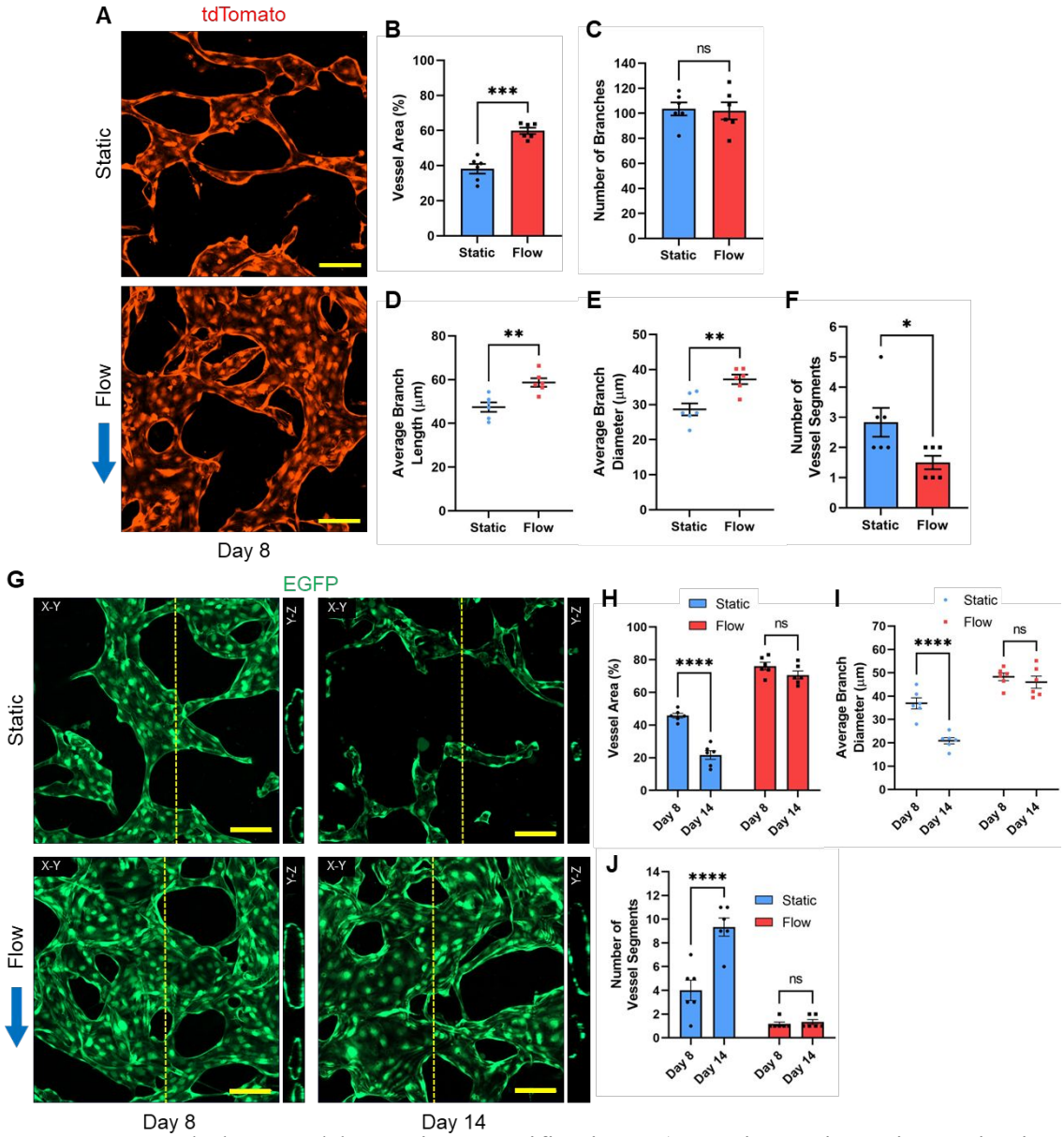

Figure 5. MVN morphology and longevity quantification. A) Maximum intensity projection of fluorescence confocal images of microvessels (tdTomato, red) cultured under static and flow conditions for 8 days. PCs and ACs were not labeled. B-F) Graphs comparing the vessel area (B), number of branches (C), average branch length (D), average branch diameter (E), and number of vessel segments (F) between MVNs cultured under static and flow conditions. G) Fluorescence confocal images of microvessels (EGFP, green) cultured under static and flow conditions for 8 and 14 days. Images show the maximum intensity projection of the X-Y plane and the cross-section of the Y-Z plane at the yellow dashed line. PCs and ACs were not labeled. H-J) Graphs comparing the vessel area (H), average branch diameter (I), and the number of vessel segments (J) between Day 8 and Day 14 for MVNs cultured under static and flow conditions. A, H) Blue arrows indicate direction of interstitial flow. Scale bars indicate 100 μm. B-F, H-J) The data show mean value, error bars ± SEM, n = 6, ns $p > 0.05$, * $p < 0.05$, ** $p < 0.01$, *** $p < 0.001$, **** $p < 0.0001$.

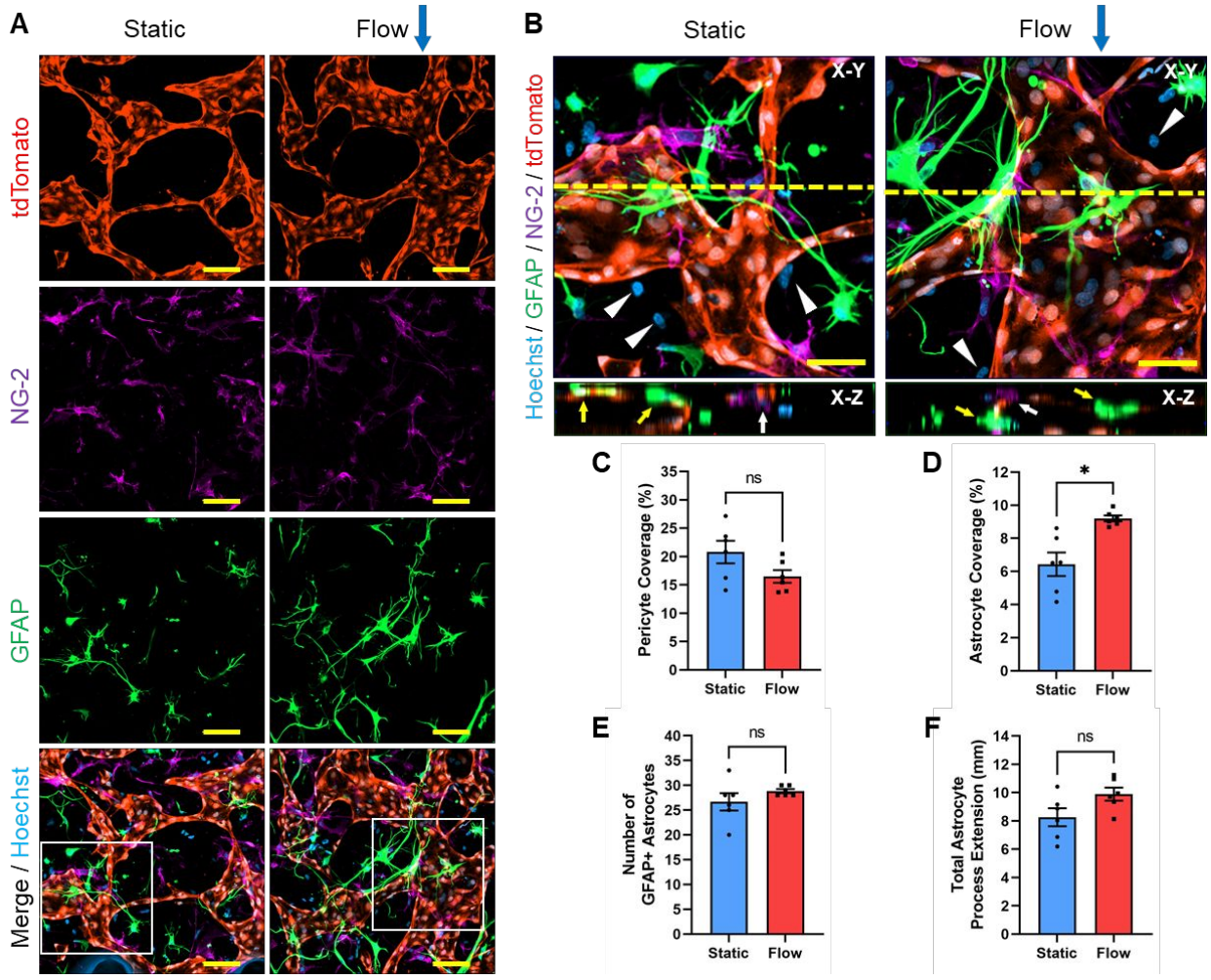

Figure 6. PC and AC microvessel coverage quantification. A) Maximum intensity projection of fluorescence confocal images of MVNs, comprised of BECs (tdTomato, red), PCs (NG-2, purple), and ACs (GFAP, green), formed under static and flow conditions on Day 8. Bottom two images show merged signals with cell nuclei (Hoechst, blue). Scale bars indicate 100 μm. B) Expanded view of white square. Images show the maximum intensity projection of the X-Y plane and the cross-section of the X-Z plane at the yellow dashed line. White triangles point to nuclei (Hoechst, blue) of cells that do not express tdTomato (red), NG-2 (purple), or GFAP (green). White and yellow arrows highlight NG-2+ PC and GFAP+ AC contact with microvessels, respectively. Scale bars indicate 50 μm. A, B) Blue arrows indicate direction of interstitial flow. C, D) Graph of the PC (C) and AC (D) coverage as a percentage of the total microvessel area measured for samples with BECs-tdT, PCs, and ACs cultured under static and flow conditions. E, F) Graphs of the number of GFAP+ nuclei (E) and the total length of astrocytic process extensions (F) measured for samples with BECs-tdT, PCs, and ACs cultured under static and flow conditions (per area). C-F) The data show mean value, error bars ± SEM, n = 6, ns $p > 0.05$, * $p < 0.05$.

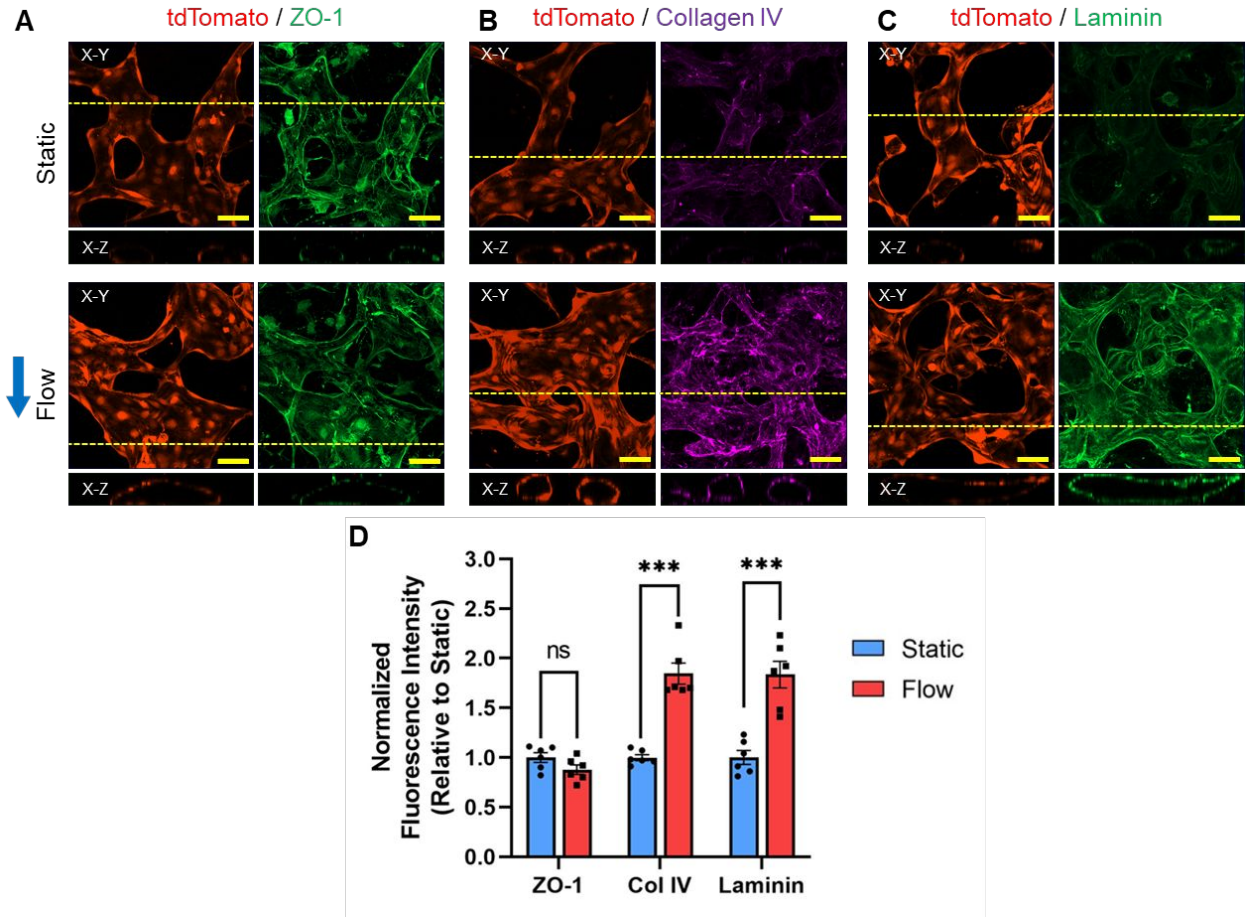

Figure 7. Immunocytochemistry analysis of BEC proteins. A, B, C) Fluorescence confocal images of microvessels (tdTomato, red) cultured under static and flow conditions stained for ZO-1 (A, green), collagen IV (B, purple), and laminin (C, green) on Day 8. Images show the maximum intensity projection of the X-Y plane and the cross-section of the X-Z plane at the yellow dashed line. Blue arrow indicates direction of interstitial flow. Scale bars indicate 50 μm. D) Graph of fluorescence intensity of ZO-1, collagen IV, and laminin identified on microvessels cultured under static and flow conditions. Total fluorescence intensity was normalized to the vessel area and presented relative to the static condition mean. The data show mean value, error bars ± SEM, n = 6, ns $p > 0.05$, *** $p < 0.001$.

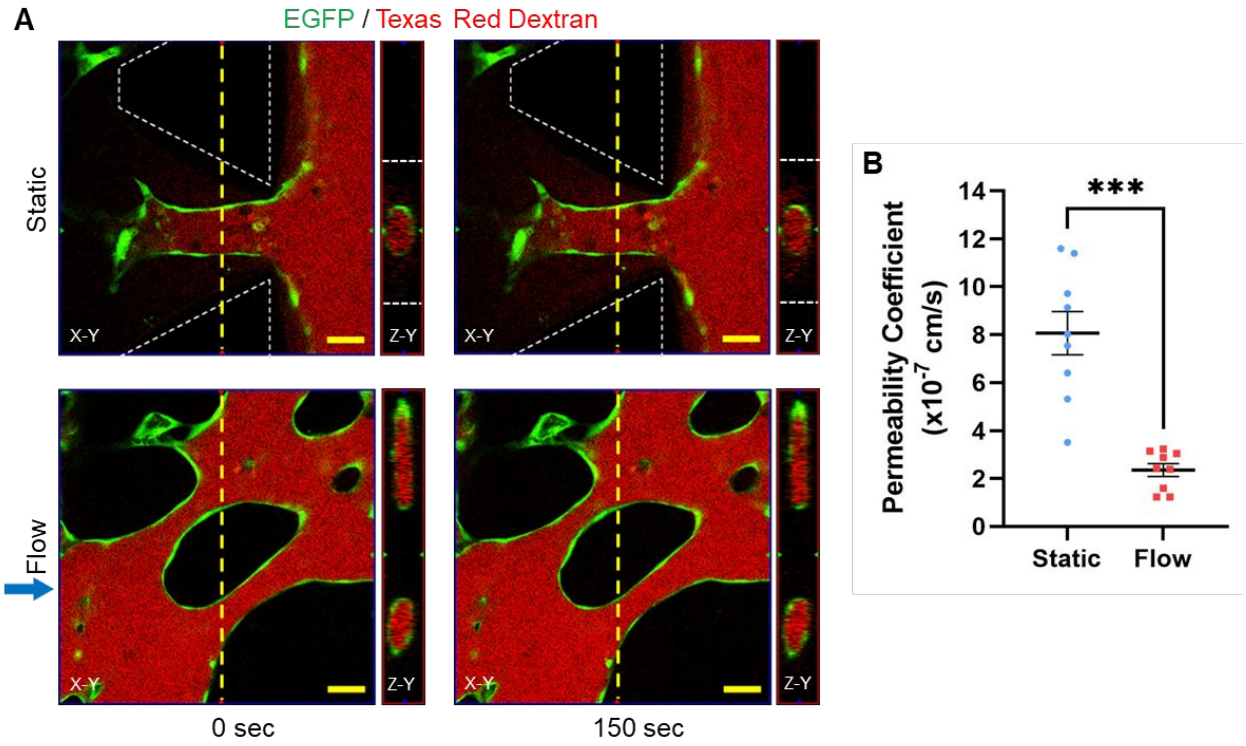

Figure 8. Dextran permeability assay. A) Fluorescence time-lapse confocal images of microvessels (EGFP, green) cultured under static and flow conditions perfused with Texas Red 70 kDa dextran (red) at 0 and 150 seconds. Images show the X-Y plane and the cross-section of the Z-Y plane at the yellow dashed line. Blue arrow indicates direction of interstitial flow. White dashed lines outline microposts. Scale bars indicate 50 μm. B) Graph of the permeability coefficient of 70kDa dextran for microvessels cultured under static and flow conditions. The data show mean value, error bars ± SEM, n = 9, *** $p < 0.001$.

Table 1. Hydrostatic Pressure Differences		
Pressure Difference (mmH_2O)	**Volume of dextran solution in high-pressure reservoirs (µL)**	**Volume of EGM-2 in low-pressure reservoirs (µL)**
0	60	60
0.375	65	55
0.75	70	50
1.125	75	45
1.5	80	40

References

1. Abbott NJ, Patabendige AAK, Dolman DEM, Yusof SR, Begley DJ. Structure and function of the blood–brain barrier. Neurobiol Dis [Internet]. 2010 Jan 1 [cited 2019 Mar 31];37(1):13–25. Available from: https://www.sciencedirect.com/science/article/pii/S0969996109002083
2. Armulik A, Genové G, Mäe M, Nisancioglu MH, Wallgard E, Niaudet C, et al. Pericytes regulate the blood–brain barrier. Nature [Internet]. 2010 Nov 25 [cited 2017 Oct 16];468(1):557–61. Available from: http://www.nature.com/doifinder/10.1038/nature09522
3. Hamilton NB, Attwell D, Hall CN. Pericyte-mediated regulation of capillary diameter: a component of neurovascular coupling in health and disease. Front Neuroenergetics [Internet]. 2010 May 21 [cited 2017 Oct 19];2(5):5. Available from: http://www.ncbi.nlm.nih.gov/pubmed/20725515
4. Abbott NJ, Rönnbäck L, Hansson E. Astrocyte–endothelial interactions at the blood–brain barrier. Nat Rev Neurosci [Internet]. 2006 Jan [cited 2017 May 23];7(1):41–53. Available from: http://www.nature.com/doifinder/10.1038/nrn1824
5. Kelleher RJ, Soiza RL. Evidence of endothelial dysfunction in the development of Alzheimer's disease: Is Alzheimer's a vascular disorder? Am J Cardiovasc Dis [Internet]. 2013 Nov 1 [cited 2019 Mar 31];3(4):197–226. Available from: http://www.ncbi.nlm.nih.gov/pubmed/24224133
6. Kortekaas R, Leenders KL, van Oostrom JCH, Vaalburg W, Bart J, Willemsen ATM, et al. Blood-brain barrier dysfunction in parkinsonian midbrain in vivo. Ann Neurol [Internet]. 2005 Feb [cited 2019 Mar 31];57(2):176–9. Available from: http://doi.wiley.com/10.1002/ana.20369
7. Drouin-Ouellet J, Sawiak SJ, Cisbani G, Lagacé M, Kuan W-L, Saint-Pierre M, et al. Cerebrovascular and blood-brain barrier impairments in Huntington's disease: Potential implications for its pathophysiology. Ann Neurol [Internet]. 2015 Aug [cited 2019 Mar 31];78(2):160–77. Available from: http://www.ncbi.nlm.nih.gov/pubmed/25866151
8. Haller E, Saporta S, Nicosia S V, Sanberg P. Ultrastructure of blood-brain barrier and blood-spinal cord barrier in SOD1 mice modeling ALS. Brain Res [Internet]. 2007 [cited 2019 Mar 31];126–37. Available from: https://www.researchgate.net/publication/6319424
9. Sandoval KE, Witt KA. Blood-brain barrier tight junction permeability and ischemic stroke. Neurobiol Dis [Internet]. 2008 Nov 1 [cited 2019 Mar 31];32(2):200–19. Available from: https://www.sciencedirect.com/science/article/pii/S0969996108001927?via%3Dihub
10. Wilhelm I, Molnár J, Fazakas C, Haskó J, Krizbai IA. Role of the blood-brain barrier in the formation of brain metastases. Int J Mol Sci [Internet]. 2013 Jan 11 [cited 2019 Mar 31];14(1):1383–411. Available from: http://www.ncbi.nlm.nih.gov/pubmed/23344048
11. Pardridge WM. The blood-brain barrier: bottleneck in brain drug development. NeuroRx [Internet]. 2005 Jan [cited 2017 Oct 20];2(1):3–14. Available from: http://www.ncbi.nlm.nih.gov/pubmed/15717053
12. Kaisar MA, Sajja RK, Prasad S, Abhyankar V V, Liles T, Cucullo L. New experimental models of the blood-brain barrier for CNS drug discovery. Expert Opin Drug Discov [Internet]. 2017 Jan [cited 2019 Apr 1];12(1):89–103. Available from: http://www.ncbi.nlm.nih.gov/pubmed/27782770
13. Booth R, Kim H. Characterization of a microfluidic in vitro model of the blood-brain

barrier (μBBB). Lab Chip [Internet]. 2012 [cited 2017 May 2];12(10):1784. Available from: http://xlink.rsc.org/?DOI=c2lc40094d
14. Griep LM, Wolbers F, de Wagenaar B, Ter Braak PM, Weksler BB, Romero IA, et al. BBB on CHIP: Microfluidic platform to mechanically and biochemically modulate blood-brain barrier function. Biomed Microdevices [Internet]. 2013 Feb 6 [cited 2017 Apr 20];15(1):145–50. Available from: http://link.springer.com/10.1007/s10544-012-9699-7
15. Wang YI, Abaci HE, Shuler ML. Microfluidic blood–brain barrier model provides in vivo-like barrier properties for drug permeability screening. Biotechnol Bioeng [Internet]. 2017 Jan [cited 2017 Apr 20];114(1):184–94. Available from: http://doi.wiley.com/10.1002/bit.26045
16. Campisi M, Shin Y, Osaki T, Hajal C, Chiono V, Kamm RD. 3D self-organized microvascular model of the human blood-brain barrier with endothelial cells, pericytes and astrocytes. Biomaterials [Internet]. 2018 Oct 1 [cited 2018 Jul 30];180:117–29. Available from: https://www.sciencedirect.com/science/article/pii/S0142961218304915#mmc1
17. Lee S, Chung M, Jeon NL. 3D brain angiogenesis model to reconstitute maturation of functional human blood-brain barrier in vitro. bioRxiv [Internet]. 2018 Nov 18 [cited 2019 Mar 31];471334. Available from: https://www.biorxiv.org/content/10.1101/471334v1
18. Braverman IM. The cutaneous microcirculation. In: Journal of Investigative Dermatology Symposium Proceedings [Internet]. Blackwell Publishing Inc.; 2000 [cited 2021 May 25]. p. 3–9. Available from: http://www.jidsponline.org/article/S0022202X15528510/fulltext
19. Marín-Padilla M. The human brain intracerebral microvascular system: Development and structure. Front Neuroanat [Internet]. 2012 Sep 13 [cited 2021 May 25];6(SEPTEMBER):1–14. Available from: www.frontiersin.org
20. Shi ZD, Ji XY, Qazi H, Tarbell JM. Interstitial flow promotes vascular fibroblast, myofibroblast, and smooth muscle cell motility in 3-D collagen I via upregulation of MMP-1. Am J Physiol - Hear Circ Physiol [Internet]. 2009 Oct [cited 2021 May 24];297(4):H1225. Available from: /pmc/articles/PMC2770759/
21. Shi ZD, Ji XY, Berardi DE, Qazi H, Tarbell JM. Interstitial flow induces MMP-1 expression and vascular SMC migration in collagen I gels via an ERK1/2-dependent and c-Jun-mediated mechanism. Am J Physiol - Hear Circ Physiol [Internet]. 2010 Jan [cited 2021 May 24];298(1):H127. Available from: /pmc/articles/PMC2806139/
22. Shirure VS, Lezia A, Tao A, Alonzo LF, George SC. Low levels of physiological interstitial flow eliminate morphogen gradients and guide angiogenesis. Angiogenesis [Internet]. 2017 Nov 12 [cited 2019 Apr 2];20(4):493–504. Available from: http://link.springer.com/10.1007/s10456-017-9559-4
23. Abe Y, Watanabe M, Chung S, Kamm RD, Tanishita K, Sudo R. Balance of interstitial flow magnitude and vascular endothelial growth factor concentration modulates three-dimensional microvascular network formation. APL Bioeng [Internet]. 2019 Sep 1 [cited 2021 May 25];3(3):36102. Available from: /pmc/articles/PMC6697031/
24. Moya ML, Hsu Y-H, Lee AP, Hughes CCW, George SC. In Vitro Perfused Human Capillary Networks. Tissue Eng Part C Methods [Internet]. 2013;19(9):730–7. Available from: http://online.liebertpub.com/doi/abs/10.1089/ten.tec.2012.0430
25. Hsu Y-H, Moya ML, Hughes CCW, Georgea SC, Lee AP. A microfluidic platform for generating large-scale nearly identical human microphysiological system arrays. Lab Chip. 2013;13(15):2990–8.

26. Alonzo LF, Moya ML, Shirure VS, George SC. Microfluidic device to control interstitial flow-mediated homotypic and heterotypic cellular communication. Lab Chip [Internet]. 2015;15:3521–9. Available from: http://pubs.rsc.org/en/Content/ArticleLanding/2015/LC/C5LC00507H
27. Boardman KC, Swartz MA, KC B, MA S. Interstitial flow as a guide for lymphangiogenesis. Circ Res [Internet]. 2003 Apr 18 [cited 2021 May 25];92(7):801–8. Available from: https://pubmed.ncbi.nlm.nih.gov/12623882/
28. Wiig H, Swartz MA. Interstitial fluid and lymph formation and transport: Physiological regulation and roles in inflammation and cancer [Internet]. Vol. 92, Physiological Reviews. American Physiological Society Bethesda, MD; 2012 [cited 2021 May 25]. p. 1005–60. Available from: www.prv.org
29. Ng CP, Helm C-LE, Swartz MA. Interstitial flow differentially stimulates blood and lymphatic endothelial cell morphogenesis in vitro. Microvasc Res [Internet]. 2004 Nov 1 [cited 2019 Apr 1];68(3):258–64. Available from: https://www.sciencedirect.com/science/article/pii/S0026286204001128?via%3Dihub#bib17
30. Tarbell JM, Shi ZD. Effect of the glycocalyx layer on transmission of interstitial flow shear stress to embedded cells. Biomech Model Mechanobiol [Internet]. 2013 Jan [cited 2021 May 25];12(1):111–21. Available from: https://pubmed.ncbi.nlm.nih.gov/22411016/
31. Rutkowski JM, Swartz MA. A driving force for change: interstitial flow as a morphoregulator. Vol. 17, Trends in Cell Biology. Elsevier Current Trends; 2007. p. 44–50.
32. Polacheck WJ, Charest JL, Kamm RD. Interstitial flow influences direction of tumor cell migration through competing mechanisms. Proc Natl Acad Sci U S A [Internet]. 2011 Jul 5 [cited 2021 May 25];108(27). Available from: /pmc/articles/PMC3131352/
33. Swartz MA, Lund AW. Lymphatic and interstitial flow in the tumour microenvironment: Linking mechanobiology with immunity [Internet]. Vol. 12, Nature Reviews Cancer. Nature Publishing Group; 2012 [cited 2021 May 25]. p. 210–9. Available from: www.nature.com/reviews/cancer
34. Ng CP, Hinz B, Swartz MA. Interstitial fluid flow induces myofibroblast differentiation and collagen alignment in vitro. J Cell Sci [Internet]. 2005 Oct 15 [cited 2021 May 25];118(20):4731–9. Available from: https://pubmed.ncbi.nlm.nih.gov/16188933/
35. Swartz MA, Fleury ME. Interstitial flow and its effects in soft tissues [Internet]. Vol. 9, Annual Review of Biomedical Engineering. Annual Reviews; 2007 [cited 2021 May 19]. p. 229–56. Available from: https://www.annualreviews.org/doi/abs/10.1146/annurev.bioeng.9.060906.151850
36. Shetty AK, Zanirati G. The Interstitial System of the Brain in Health and Disease [Internet]. Aging and Disease Feb 1, 2020. Available from: /pmc/articles/PMC6961771/
37. Jessen NA, Munk ASF, Lundgaard I, Nedergaard M. The Glymphatic System – A Beginner's Guide. Neurochem Res [Internet]. 2015 Dec 1 [cited 2021 Sep 14];40(12):2583. Available from: /pmc/articles/PMC4636982/
38. Griffith LG, Swartz MA. Capturing complex 3D tissue physiology in vitro [Internet]. Vol. 7, Nature Reviews Molecular Cell Biology. Nature Publishing Group; 2006 [cited 2021 May 24]. p. 211–24. Available from: www.nature.com/reviews/molcellbio
39. Helm CLE, Fleury ME, Zisch AH, Boschetti F, Swartz MA. Synergy between interstitial flow and VEGF directs capillary morphogenesis in vitro through a gradient amplification

mechanism. Proc Natl Acad Sci U S A [Internet]. 2005 Nov 1 [cited 2021 Jun 23];102(44):15779–84. Available from: /pmc/articles/PMC1276047/
40. Kim S, Chung M, Ahn J, Lee S, Jeon NL. Interstitial flow regulates the angiogenic response and phenotype of endothelial cells in a 3D culture model. Lab Chip [Internet]. 2016 Oct 18 [cited 2021 Jun 21];16(21):4189–99. Available from: http://fiji.sc/Fiji
41. Hsu Y, Moya M, Abiri P, Hughes C. Full range physiological mass transport control in 3D tissue cultures. Lab Chip [Internet]. 2013;13(1):81–9. Available from: http://www.pubmedcentral.nih.gov/articlerender.fcgi?artid=3510322&tool=pmcentrez&rendertype=abstract%5Cnhttp://pubs.rsc.org/en/content/articlehtml/2013/lc/c2lc40787f
42. Tinken TM, Thijssen DHJ, Hopkins N, Black MA, Dawson EA, Minson CT, et al. Impact of shear rate modulation on vascular function in humans. Hypertension [Internet]. 2009 Aug [cited 2021 May 25];54(2):278–85. Available from: /pmc/articles/PMC3012006/
43. Lu D, Kassab GS. Role of shear stress and stretch in vascular mechanobiology [Internet]. Vol. 8, Journal of the Royal Society Interface. Royal Society; 2011 [cited 2021 May 25]. p. 1379–85. Available from: /pmc/articles/PMC3163429/
44. McCormick SM, Eskin SG, McIntire L V., Teng CL, Lu CM, Russell CG, et al. DNA microarray reveals changes in gene expression of shear stressed human umbilical vein endothelial cells. Proc Natl Acad Sci U S A [Internet]. 2001 Jul 31 [cited 2021 May 24];98(16):8955–60. Available from: /pmc/articles/PMC55355/
45. Topper JN, Gimbrone MA. Blood flow and vascular gene expression: fluid shear stress as a modulator of endothelial phenotype. Mol Med Today. 1999 Jan 1;5(1):40–6.
46. Cucullo L, Hossain M, Puvenna V, Marchi N, Janigro D. The role of shear stress in Blood-Brain Barrier endothelial physiology. BMC Neurosci [Internet]. 2011 May 11 [cited 2017 Sep 11];12(40):1471–2202. Available from: http://www.biomedcentral.com/1471-2202/12/40
47. Figarol A, Piantino M, Furihata T, Satoh T, Sugiura S, Kanamori T, et al. Interstitial flow regulates in vitro three-dimensional self-organized brain micro-vessels. Biochem Biophys Res Commun [Internet]. 2020 Dec 10 [cited 2021 Feb 15];533(3):600–6. Available from: https://doi.org/10.1016/j.bbrc.2020.09.061
48. Wang W, Dentler WL, Borchardt RT. VEGF increases BMEC monolayer permeability by affecting occludin expression and tight junction assembly. Am J Physiol - Hear Circ Physiol [Internet]. 2001 [cited 2021 Apr 27];280(1 49-1). Available from: http://www.ajpheart.org
49. Uwamori H, Ono Y, Yamashita T, Arai K, Sudo R. Comparison of organ-specific endothelial cells in terms of microvascular formation and endothelial barrier functions. Microvasc Res [Internet]. 2019 Mar 1 [cited 2021 Feb 16];122:60–70. Available from: /pmc/articles/PMC6294313/
50. Li Y, Pi Q-MM, Wang P-CC, Liu L-JJ, Han Z-GG, Shao Y, et al. Functional human 3D microvascular networks on a chip to study the procoagulant effects of ambient fine particulate matter. RSC Adv [Internet]. 2017 Dec 12 [cited 2018 Apr 2];7(88):56108–16. Available from: https://pubs.rsc.org/en/content/articlehtml/2017/ra/c7ra11357a
51. Kim S, Lee H, Chung M, Jeon NL. Engineering of functional, perfusable 3D microvascular networks on a chip. Lab Chip [Internet]. 2013;13(8):1489–500. Available from: http://www.ncbi.nlm.nih.gov/pubmed/23440068
52. Kimelberg HK. The problem of astrocyte identity. Neurochem Int. 2004 Jul 1;45(2–3):191–202.

53. Oberheim NA, Goldman SA, Nedergaard M. Heterogeneity of astrocytic form and function. Methods Mol Biol [Internet]. 2012 [cited 2021 Apr 6];814:23–45. Available from: /pmc/articles/PMC3506190/
54. Buchanan CF, Verbridge SS, Vlachos PP, Rylander MN. Flow shear stress regulates endothelial barrier function and expression of angiogenic factors in a 3D microfluidic tumor vascular model. Cell Adhes Migr [Internet]. 2014 Sep 1 [cited 2021 Jan 21];8(5):517–24. Available from: /pmc/articles/PMC4594487/
55. Goldberg JS, Hirschi KK. A Vascular Perspective on Neurogenesis. In: Neural Stem Cells - New Perspectives [Internet]. InTech; 2013 [cited 2017 Aug 31]. p. 201–39. Available from: http://www.intechopen.com/books/neural-stem-cells-new-perspectives/a-vascular-perspective-on-neurogenesis
56. Marie C, Pedard M, Quirié A, Tessier A, Garnier P, Totoson P, et al. Brain-derived neurotrophic factor secreted by the cerebral endothelium: A new actor of brain function? [Internet]. Vol. 38, Journal of Cerebral Blood Flow and Metabolism. SAGE Publications Ltd; 2018 [cited 2021 Feb 8]. p. 935–49. Available from: /pmc/articles/PMC5998997/
57. Gaceb A, Özen I, Padel T, Barbariga M, Paul G. Pericytes secrete pro-regenerative molecules in response to platelet-derived growth factor-BB. J Cereb Blood Flow Metab [Internet]. 2018 Jan 1 [cited 2021 Apr 15];38(1):45–57. Available from: http://journals.sagepub.com/doi/10.1177/0271678X17719645
58. Fernández-García S, Sancho-Balsells A, Longueville S, Hervé D, Gruart A, Delgado-García JM, et al. Astrocytic BDNF and TrkB regulate severity and neuronal activity in mouse models of temporal lobe epilepsy. Cell Death Dis [Internet]. 2020 Jun 1 [cited 2021 Apr 15];11(6):1–17. Available from: https://doi.org/10.1038/s41419-020-2615-9
59. Xiao Y, Kim D, Dura B, Zhang K, Yan R, Li H, et al. Ex vivo dynamics of human glioblastoma cells in a microvasculature-on-a-chip system correlates with tumor heterogeneity and subtypes. Adv Sci [Internet]. 2019 Apr 17 [cited 2018 Sep 10];6(8):1801531. Available from: http://dx.doi.org/10.1101/400739
60. Xiao Y, Liu C, Chen Z, Blatchley MR, Kim D, Zhou J, et al. Senescent Cells with Augmented Cytokine Production for Microvascular Bioengineering and Tissue Repairs. Adv Biosyst [Internet]. 2019 Aug 1 [cited 2021 Jun 22];3(8):1900089. Available from: www.adv-biosys.com
61. Adriani G, Ma D, Pavesi A, Kamm RD, Goh ELK, Neuwelt EA, et al. A 3D neurovascular microfluidic model consisting of neurons, astrocytes and cerebral endothelial cells as a blood–brain barrier. Lab Chip [Internet]. 2017;12:169–82. Available from: http://xlink.rsc.org/?DOI=C6LC00638H
62. Park T-E, Mustafaoglu N, Herland A, Hasselkus RM, Mannix R, FitzGerald EA, et al. Hypoxia-enhanced Blood-Brain Barrier Chip recapitulates human barrier function, drug penetration, and antibody shuttling properties. bioRxiv [Internet]. 2018 Nov 29 [cited 2019 Mar 4];482463. Available from: https://www.biorxiv.org/content/10.1101/482463v1
63. Vatine GD, Barrile R, Workman MJ, Sances S, Barriga BK, Rahnama M, et al. Human iPSC-Derived Blood-Brain Barrier Chips Enable Disease Modeling and Personalized Medicine Applications. Cell Stem Cell. 2019 Jun 6;24(6):995-1005.e6.
64. Ahn SI, Sei YJ, Park HJ, Kim J, Ryu Y, Choi JJ, et al. Microengineered human blood–brain barrier platform for understanding nanoparticle transport mechanisms. Nat Commun [Internet]. 2020 Dec 1 [cited 2020 Oct 27];11(1):1–12. Available from: https://doi.org/10.1038/s41467-019-13896-7

65. Vickerman V, Kamm RD. Mechanism of a flow-gated angiogenesis switch: early signaling events at cell–matrix and cell–cell junctions. Integr Biol [Internet]. 2012 Jul 23 [cited 2021 Sep 8];4(8):863–74. Available from: https://academic.oup.com/ib/article/4/8/863/5204448
66. Chary SR, Jain RK. Direct measurement of interstitial convection and diffusion of albumin in normal and neoplastic tissues by fluorescence photobleaching. Proc Natl Acad Sci U S A [Internet]. 1989 [cited 2021 Jun 30];86(14):5385–9. Available from: /pmc/articles/PMC297627/?report=abstract
67. Kingsmore KM, Vaccari A, Abler D, Cui SX, Epstein FH, Rockne RC, et al. MRI analysis to map interstitial flow in the brain tumor microenvironment. APL Bioeng [Internet]. 2018 Sep 1 [cited 2021 Feb 26];2(3):31905. Available from: https://doi.org/10.1063/1.5023503
68. Byun CK, Abi-Samra K, Cho YK, Takayama S. Pumps for microfluidic cell culture. Vol. 35, Electrophoresis. Wiley-VCH Verlag; 2014. p. 245–57.
69. Bergers G, Song S. The role of pericytes in blood-vessel formation and maintenance [Internet]. Vol. 7, Neuro-Oncology. Oxford University Press; 2005 [cited 2021 May 19]. p. 452–64. Available from: /pmc/articles/PMC1871727/
70. Biswas S, Cottarelli A, Agalliu D. Neuronal and glial regulation of CNS angiogenesis and barriergenesis [Internet]. Vol. 147, Development (Cambridge). Company of Biologists Ltd; 2020 [cited 2021 May 19]. Available from: /pmc/articles/PMC7197727/
71. Song JW, Munn LL. Fluid forces control endothelial sprouting. Proc Natl Acad Sci U S A [Internet]. 2011 Sep 13 [cited 2019 Apr 4];108(37):15342–7. Available from: http://www.ncbi.nlm.nih.gov/pubmed/21876168
72. Vilanova G, Burés M, Colominas I, Gomez H. Computational modelling suggests complex interactions between interstitial flow and tumour angiogenesis. J R Soc Interface [Internet]. 2018 Sep 1 [cited 2021 Sep 8];15(146). Available from: https://royalsocietypublishing.org/doi/abs/10.1098/rsif.2018.0415
73. Ballermann BJ, Dardik A, Eng E, Liu A. Shear stress and the endothelium. In: Kidney International, Supplement. Nature Publishing Group; 1998. p. S100–8.
74. Park JY, White JB, Walker N, Kuo CH, Cha W, Meyerhoff ME, et al. Responses of endothelial cells to extremely slow flows. Biomicrofluidics [Internet]. 2011 [cited 2021 Jan 21];5(2). Available from: /pmc/articles/PMC3145236/?report=abstract
75. Ohura N, Yamamoto K, Ichioka S, Sokabe T, Nakatsuka H, Baba A, et al. Global Analysis of Shear Stress-Responsive Genes in Vascular Endothelial Cells. Vol. 304, Journal of Atherosclerosis and Thrombosis Original Articles.
76. Jeon JS, Bersini S, Whisler JA, Chen MB, Dubini G, Charest JL, et al. Generation of 3D functional microvascular networks with human mesenchymal stem cells in microfluidic systems. Integr Biol (Camb) [Internet]. 2014 May [cited 2017 Apr 19];6(5):555–63. Available from: http://www.ncbi.nlm.nih.gov/pubmed/24676392
77. Papaioannou TG, Stefanadis C. Vascular wall shear stress: Basic principles and methods [Internet]. Vol. 46, Hellenic Journal of Cardiology. 2005 [cited 2021 May 20]. p. 9–15. Available from: https://europepmc.org/article/med/15807389
78. Loufrani L, Henrion D. Role of the cytoskeleton in flow (shear stress)-induced dilation and remodeling in resistance arteries. Med Biol Eng Comput [Internet]. 2008 May [cited 2021 May 20];46(5):451–60. Available from: /pmc/articles/PMC2566739/
79. Osborn EA, Rabodzey A, Dewey CF, Hartwig JH. Endothelial actin cytoskeleton remodeling during mechanostimulation with fluid shear stress. Am J Physiol - Cell

Physiol [Internet]. 2006 Feb [cited 2021 May 20];290(2):444–52. Available from: www.ajpcell.org
80. Korn C, Augustin HG. Mechanisms of Vessel Pruning and Regression. Vol. 34, Developmental Cell. Cell Press; 2015. p. 5–17.
81. Bhalerao A, Sivandzade F, Archie SR, Chowdhury EA, Noorani B, Cucullo L. In vitro modeling of the neurovascular unit: Advances in the field [Internet]. Vol. 17, Fluids and Barriers of the CNS. BioMed Central Ltd.; 2020 [cited 2020 Oct 27]. p. 22. Available from: https://doi.org/10.1186/s12987-020-00183-7
82. Slanzi A, Iannoto G, Rossi B, Zenaro E, Constantin G. In vitro Models of Neurodegenerative Diseases [Internet]. Vol. 8, Frontiers in Cell and Developmental Biology. Frontiers Media S.A.; 2020 [cited 2021 Jun 22]. p. 328. Available from: www.frontiersin.org
83. Rasmussen MK, Mestre H, Nedergaard M. The glymphatic pathway in neurological disorders. Lancet Neurol [Internet]. 2018 Nov 1 [cited 2021 Oct 7];17(11):1016. Available from: /pmc/articles/PMC6261373/
84. Wragg JW, Durant S, Mcgettrick HM, Sample KM, Egginton S, Bicknell R. Shear stress regulated gene expression and angiogenesis in vascular endothelium [Internet]. Vol. 21, Microcirculation. Blackwell Publishing Ltd; 2014 [cited 2021 May 24]. p. 290–300. Available from: https://onlinelibrary.wiley.com/doi/full/10.1111/micc.12119
85. Colgan OC, Ferguson G, Collins NT, Murphy RP, Meade G, Cahill PA, et al. Regulation of bovine brain microvascular endothelial tight junction assembly and barrier function by laminar shear stress. Am J Physiol Circ Physiol [Internet]. 2007 Jun [cited 2021 Feb 8];292(6):H3190–7. Available from: https://www.physiology.org/doi/10.1152/ajpheart.01177.2006
86. DeStefano JG, Xu ZS, Williams AJ, Yimam N, Searson PC. Effect of shear stress on iPSC-derived human brain microvascular endothelial cells (dhBMECs). Fluids Barriers CNS [Internet]. 2017 Aug 4 [cited 2021 May 3];14(1):20. Available from: http://fluidsbarrierscns.biomedcentral.com/articles/10.1186/s12987-017-0068-z
87. Yamane T, Mitsumata M, Yamaguchi N, Nakazawa T, Mochizuki K, Kondo T, et al. Laminar high shear stress up-regulates type IV collagen synthesis and down-regulates MMP-2 secretion in endothelium. A quantitative analysis. Cell Tissue Res [Internet]. 2010 Jun 20 [cited 2021 Feb 8];340(3):471–9. Available from: https://link.springer.com/article/10.1007/s00441-010-0968-6
88. Yamane T, Yamaguchi N, Yoshida Y, Mitsumata M. Regulation of extracellular matrix production and degradation of endothelial cells by shear stress. Int Congr Ser. 2004 May 1;1262(C):407–10.
89. Béguin EP, Janssen EFJ, Hoogenboezem M, Meijer AB, Hoogendijk AJ, van den Biggelaar M. Flow-induced Reorganization of Laminin-integrin Networks Within the Endothelial Basement Membrane Uncovered by Proteomics. Mol Cell Proteomics. 2020 Jul 1;19(7):1179–92.
90. Di Russo J, Luik A-LA, Yousif L, Budny S, Oberleithner H, Hofschröer V, et al. Endothelial basement membrane laminin 511 is essential for shear stress response. EMBO J [Internet]. 2017 Jan 17 [cited 2021 Feb 8];36(2):183–201. Available from: https://onlinelibrary.wiley.com/doi/10.15252/embj.201694756
91. Virgintino D, Robertson D, Monaghan P, Errede M, Bertossi M, Ambrosi G, et al. Glucose transporter GLUT1 in human brain microvessels revealed by ultrastructural

immunocytochemistry. J Submicrosc Cytol Pathol [Internet]. 1997 [cited 2021 Oct 4];29(3):365–70. Available from: https://pubmed.ncbi.nlm.nih.gov/9267045/
92. Barathi S, Angayarkanni N, Sumantran VN. GLUT-1 Expression in Bovine Retinal Capillary Endothelial Cells and Pericytes Exposed to Advanced Glycation End Products. Invest Ophthalmol Vis Sci [Internet]. 2010 Dec 1 [cited 2021 Oct 4];51(12):6810–4. Available from: http://rsb.info.nih.gov/ij/index.html
93. Mandarino LJ, Finlayson J, Hassell J. High glucose downregulates glucose transport activity in retinal capillary pericytes but not endothelial cells. Invest Ophthalmol Vis Sci [Internet]. 1994 [cited 2021 Oct 5];35(3):964–72. Available from: https://iovs.arvojournals.org/article.aspx?articleid=2161822
94. Morgello S, Uson RR, Schwartz EJ, Haber RS. The human blood-brain barrier glucose transporter (GLUT1) is a glucose transporter of gray matter astrocytes. Glia [Internet]. 1995 May 1 [cited 2021 Oct 4];14(1):43–54. Available from: https://onlinelibrary.wiley.com/doi/full/10.1002/glia.440140107
95. Allen A, Messier C. Plastic changes in the astrocyte GLUT1 glucose transporter and beta-tubulin microtubule protein following voluntary exercise in mice. Behav Brain Res. 2013 Mar 1;240(1):95–102.
96. Bendayan R, Ronaldson PT, Gingras D, Bendayan M. In Situ Localization of P-glycoprotein (ABCB1) in Human and Rat Brain. J Histochem Cytochem [Internet]. 2006 Oct [cited 2021 Oct 4];54(10):1159. Available from: /pmc/articles/PMC3957801/
97. D V, M E, F G, C C, D R, A V, et al. Fetal blood-brain barrier P-glycoprotein contributes to brain protection during human development. J Neuropathol Exp Neurol [Internet]. 2008 Jan [cited 2021 Oct 5];67(1):50–61. Available from: https://pubmed.ncbi.nlm.nih.gov/18091560/
98. Ronaldson PT, Bendayan M, Gingras D, Piquette-Miller M, Bendayan R. Cellular localization and functional expression of P-glycoprotein in rat astrocyte cultures. J Neurochem [Internet]. 2004 May 1 [cited 2021 Oct 5];89(3):788–800. Available from: https://onlinelibrary.wiley.com/doi/full/10.1111/j.1471-4159.2004.02417.x
99. X W, S H, Y J, Y L, T S, D L, et al. Reactive astrocytes increase the expression of P-gp and Mrp1 via TNF-α and NF-κB signaling. Mol Med Rep [Internet]. 2018 Jan 1 [cited 2021 Oct 5];17(1):1198–204. Available from: https://pubmed.ncbi.nlm.nih.gov/29115482/
100. Callaghan R, Luk F, Bebawy M. Inhibition of the Multidrug Resistance P-Glycoprotein: Time for a Change of Strategy? Drug Metab Dispos [Internet]. 2014 [cited 2021 Oct 5];42(4):623. Available from: /pmc/articles/PMC3965902/
101. Burghoff S, Schrader J. Secretome of human endothelial cells under shear stress. J Proteome Res [Internet]. 2011 Mar 4 [cited 2021 Jun 23];10(3):1160–9. Available from: http://www.expasy.org/sprot
102. Li G, Simon MJ, Cancel LM, Shi Z-D, Xinying Ji JM, Tarbell, Barclay Morrison III and BMF. Permeability of Endothelial and Astrocyte Cocultures: In Vitro Blood–Brain Barrier Models for Drug Delivery Studies. 2012;76(October 2009):211–20.
103. Biemans EALM, Jäkel L, de Waal RMW, Kuiperij HB, Verbeek MM. Limitations of the hCMEC/D3 cell line as a model for Aβ clearance by the human blood-brain barrier. J Neurosci Res [Internet]. 2017 Jul 1 [cited 2021 May 24];95(7):1513–22. Available from: /pmc/articles/PMC5484315/
104. Afonso P V., Ozden S, Cumont MC, Seilhean D, Cartier L, Rezaie P, et al. Alteration of blood-brain barrier integrity by retroviral infection. PLoS Pathog [Internet]. 2008 Nov

[cited 2021 May 24];4(11):1000205. Available from: www.plospathogens.org
105. Yuan W, Lv Y, Zeng M, Fu BM. Non-invasive measurement of solute permeability in cerebral microvessels of the rat. Microvasc Res. 2009 Mar 1;77(2):166–73.
106. Bang S, Lee S-R, Ko J, Son K, Tahk D, Ahn J, et al. A Low Permeability Microfluidic Blood-Brain Barrier Platform with Direct Contact between Perfusable Vascular Network and Astrocytes. Sci Rep [Internet]. 2017 [cited 2017 Oct 10];7(8083). Available from: https://www.nature.com/articles/s41598-017-07416-0.pdf
107. Jiao H, Wang Z, Liu Y, Wang P, Xue Y. Specific Role of Tight Junction Proteins Claudin-5, Occludin, and ZO-1 of the Blood–Brain Barrier in a Focal Cerebral Ischemic Insult. J Mol Neurosci 2011 442 [Internet]. 2011 Feb 12 [cited 2021 Sep 14];44(2):130–9. Available from: https://link.springer.com/article/10.1007/s12031-011-9496-4
108. Xu L, Nirwane A, Yao Y. Basement membrane and blood-brain barrier [Internet]. Vol. 4, Stroke and Vascular Neurology. BMJ Publishing Group; 2019 [cited 2021 May 24]. p. 78–82. Available from: /pmc/articles/PMC6613871/
109. Bagchi S, Chhibber T, Lahooti B, Verma A, Borse V, Jayant RD. In-vitro blood-brain barrier models for drug screening and permeation studies: An overview [Internet]. Vol. 13, Drug Design, Development and Therapy. Dove Medical Press Ltd.; 2019 [cited 2021 May 25]. p. 3591–605. Available from: http://doi.org/10.2147/DDDT.S218708